JOURNAL OF GEOPHYSICAL RESEARCH, VOL. 106, NO. D2, PAGES 1693–1711, JANUARY 27, 2001

The Global Modeling Initiative assessment model: Application to high-speed civil transport perturbation

D. E. Kinnison,[1] P. S. Connell,[2] J. M. Rodriguez,[3] D. A. Rotman,[2] D. B. Considine,[4,5] J. Tannahill,[2] R. Ramaroson,[6] P. J. Rasch,[1] A. R. Douglass,[5] S. L. Baughcum,[7] L. Coy,[5] D. W. Waugh,[8] S. R. Kawa,[5] and M. J. Prather[9]

Abstract. The NASA Atmospheric Effects of Aviation Project (AEAP) Global Modeling Initiative (GMI) three-dimensional (3-D) chemical transport model (CTM) was applied to assess the impact of a fleet of high-speed civil transports (HSCTs) on abundances of stratospheric ozone, total inorganic nitrogen (NO_y), and H_2O. This model is specifically designed to incorporate a diversity of approaches to chemical and physical processes related to the stratosphere in a single computing framework, facilitating the analysis of model component differences, modeling intercomparison and comparison with data. A proposed HSCT fleet scenario was adopted, in which the aircraft cruise in the lower stratosphere, emitting nitrogen oxides (NO_x) and water (H_2O). The model calculated an HSCT-induced change in Northern and Southern Hemisphere total column ozone of +0.2% and +0.05%, respectively. This change is the result of a balance between an increase in local ozone below approximately 25 km and a decrease above this altitude. When compared to available NO_y observations, we find that the model consistently underestimates lower stratospheric NO_y. This discrepancy is consistent with the model bias toward less negative ozone impact, when compared to results from other models. Additional analysis also indicates that for an HSCT assessment it is equally important for a model to accurately represent the lower stratospheric concentrations of ozone and H_2O. The GMI model yields good agreement in comparisons to ozone data for present-day conditions, while H_2O is constrained by climatology as much as possible; thus no further biases would be expected from these comparisons. Uncertainties due to discrepancies in the calculated age of air compared to that derived from measurements, and of the impact of emissions on heterogeneous and polar chemistry, are difficult to evaluate at this point.

1. Introduction

In the 1970s the aeronautics industry expressed interest in designing and building a commercial fleet of supersonic transport (SST) aircraft. However, a concern arose that these aircraft flying in the stratosphere would produce significant amounts of nitrogen oxides (NO_x = NO+NO_2) that could catalytically destroy ozone [*Johnston*, 1971; *Climatic Impact Assessment Program (CIAP)*, 1974, 1975a, 1975b; *National Academy of Sciences (NAS)*, 1975]. This concern contributed to the decision not to develop a supersonic transport (SST) at that time.

In the late 1980s there was renewed interest in developing an SST for intercontinental passenger flights [e.g., *Johnston et al.*, 1989; First International Conference on Hypersonic Flight in the 21st Century, University of North Dakota, Grand Forks, September 1988]. On the basis of this renewed interest the National Aeronautics and Space Agency (NASA) created the Atmospheric Effects of Stratospheric Aircraft (AESA) project under the guidance of the High-Speed Research Program (HSRP) to assist in the scientific understanding of the impact of supersonic flight [*Prather et al.*, 1992]. The conceptual airplane, designated as a high-speed civil transport (HSCT), would transport approximately 300 passengers at Mach 2.4, with a supersonic cruise altitude between 17-20 km and a range of 5000 nautical miles [*Baughcum and Henderson*, 1995, 1998].

The NASA HSRP/AESA effort started in 1990 and was recently completed in 1999. The status of the projected HSCT impact was summarized at the beginning of the HSRP/AESA by *Johnston et al.* [1991] and *Douglass et al.* [1991]. Following these early reviews, there have been several NASA HSRP/AESA HSCT assessment reports [*Prather et al.*, 1992; *Stolarski and Wesoky*, 1993a, 1993b, 1995; *Stolarski et al.*, 1995; *Kawa et al.*, 1999]. *The Intergovernmental Panel on Climate Change* (IPCC) [1999] has also assessed HSCT ozone impact. The National Research Council (NRC) has examined the NASA assessment process [*NRC*, 1997, 1999], and the issue has been discussed within the European Commission Directorate General XII Science, Research, Development, Environment and Climate Programme [*Brasseur et al.*, 1998].

Until recently the national and international HSCT assessment exercises [*Kawa et al.*, 1999; *IPCC*, 1999] have used zonally averaged two-dimensional chemical-transport models. These models were designed for stratospheric investigations and have been evaluated by comparison with observational data and other

[1]National Center for Atmospheric Research, Boulder, Colorado.
[2]Lawrence Livermore National Laboratory, Livermore, California.
[3]University of Miami, Miami, Florida.
[4]Department of Meteorology, University of Maryland, College Park.
[5]NASA Goddard Space Flight Center, Greenbelt, Maryland.
[6]Office National d'Etudes et Recherches Aerospatiales, Paris, France.
[7]Boeing Company, Seattle, Washington.
[8]The Johns Hopkins University, Baltimore, Maryland.
[9]University of California at Irvine.

Paper number 2000JD900406.
0148-0227/01/2000JD900406$09.00

models [e.g., *Prather and Remsberg*, 1993; *Park et al.*, 1999]. Assessment studies with two-dimensional (2-D) models are considered acceptable for species with nonlocalized source emissions and long atmospheric lifetimes (e.g., CFCs). However, there is concern that these models may not be applicable for use in HSCT studies, where the source is localized in the lower stratosphere and is spatially nonuniform. This concern is due to the highly parameterized dynamics of 2-D models in the lower stratosphere and the absence of synoptic-scale exchange between the stratosphere and troposphere. Furthermore, due to the assumption of zonal symmetry, 2-D models may not correctly quantify the interaction of HSCT exhaust with Northern Hemisphere polar processes.

Three-dimensional (3-D) chemical transport models were used for the first time to assess HSCT impacts in both the NASA Assessment of the "Effects of High-Speed Aircraft in the Stratosphere" assessment report and the 1999 Intergovernmental Panel on Climate Change "Special Report on Aviation and the Global Atmosphere." The purpose of this paper is to summarize the derived HSCT impact on ozone from one of these 3-D models, the NASA Global Modeling Initiative (GMI) model. We also analyze the model results in the context of comparisons of GMI simulations with specific atmospheric measurements, and we discuss the systematic errors in the GMI results, which can be deduced from these comparisons.

2. Three-Dimensional Assessment Models

Three-dimensional models should inherently have many advantages over 2-D models in accurately representing stratospheric chemical and transport processes. For example, 3-D models should derive a better representation of wave-mean flow interactions due to mixing by planetary wave breaking in the surf zone, subtropics, and polar jet regions. Stratospheric-tropospheric exchange processes are not only three-dimensional, but occur on a spatial scale smaller than that of most current three-dimensional models. However, the three-dimensional framework has at least the potential to include a more physical representation of model processes, which can eventually offer a better representation of this exchange than can current two-dimensional models, where the exchange between the stratosphere and troposphere is a consequence of the adopted eddy diffusion coefficients and residual circulation. With the appropriate resolution, 3-D models could incorporate filamentary structures created by breaking Rossby waves, which can lead to non-diffusive, asymmetric transport across subtropical barriers. In addition, 3-D models are able to explicitly account for the nonzonal characteristics of temperature-sensitive heterogeneous processes, which are especially important at high latitudes in the polar regions. Although it is not clear whether the resolution adopted in current 3-D models (as for example, the 4° x 5° horizontal resolution adopted in this assessment) is sufficiently adequate to describe the above processes, it is clear that adoption of a three-dimensional framework is a prerequisite for improvements in our simulation of these processes.

The assessment of HSCT impacts on stratospheric ozone is inherently a 3-D problem. Historically, 3-D models have been developed primarily for climate studies and the assimilation of meteorological data. Current 3-D chemical-transport models (CTMs) used in assessment studies derive their transport fields from general circulation models (GCMs) studying climate, or data assimilation models, such as that of the NASA/Goddard Data Assimilation Office (DAO). These CTMs are referred to as "off-line" models since the GCM calculation is independent of the CTM results. Other chemical-transport models are run "on-line" with a GCM, but their current computational requirements make them impractical for assessment calculations. The evaluation of these models has emphasized comparison with meteorological observations, although comparisons with observed tracer distributions have been conducted for several CTMs [e.g., *Strahan and Mahlman,* 1994; *Rasch et al.*, 1994, 1995; *Boville*, 1995; *Waugh et al.*, 1997; *Avallone and Prather*, 1997; *Douglass et al.,* 1999; *Park et al.*, 1999]. Comparison of tracer simulations with observations offers an additional diagnostic of potential areas of improvement for the "parent" GCM, as well as in the CTM numerical algorithms and spatial/temporal resolution. As described below, these comparisons have been an important component of the Global Modeling Initiative effort [*Douglass et al.,* 1999], which has been greatly facilitated by a common platform where different model components and inputs can be incorporated.

2.1. Design and Goals of the GMI 3-D Core Model

The NASA Atmospheric Effects of Aviation Project (AEAP) Global Modeling Initiative was originally designed to provide a needed 3-D tool for the assessment of the impact of HSCTs and subsonic aircraft. However, the inherent flexibility of this model also gives it wider applicability. The goals in the ongoing design of this assessment tool are as follows: (1) The assessment model should be well-characterized and thoroughly tested against observations. (2) The model should be able to test and compare a diversity of approaches to specific processes by being able to easily swap modules containing different formulations of chemical processes, within a common framework [*Douglass et al.*, 1999]. (3) The model should be optimized for computational efficiency and be able to run on different platforms. (4) Model results should be examined by a large representation of the scientific community, thus facilitating consensus on the significance of assessment results. (5) Ultimately, the model integration could provide a unique assessment capability for other anthropogenic impacts of concern, by providing a testbed for other algorithms and intercomparisons used in assessments of those issues. The GMI model could thus become a resource that would relieve the intellectual and financial pressure for continued 3-D assessments.

The following elements of the GMI effort address these goals [*Rodriguez*, 1996]: (1) A common computing environment facilitates incorporation of different algorithms and approximations, intercomparison of results, and analysis. A core institution (Lawrence Livermore National Laboratory) is responsible for actual integration of the code, maintaining common software standard, and standardizing the code for efficient utilization of different computing platforms, including parallel architectures. Currently, the model is implemented and run on the following computational platforms: Cray J90, Cray SV1, Cray T3E, IBM SP, COMPAQ SC1, as well as desktop workstations such as Suns and SGIs. Simulation results across these platforms agree to within roundoff error. Parallel efficiency varies among these platforms between 80-90% efficient using up to 100 processors, but begins to fall off to 50-70% when using more processors. (2) A science team under a project scientist is responsible for setting the model development, scientific priorities, and analysis of results. (3) The effort continually leverages from the ongoing research by members of the scientific community, thus maintaining cutting-edge science in the model. The science team/core model combination frees up scientists from the burdens

of assessment; furthermore, it has created a structure for synergistic research among scientists in the team. At this point we have a team of about 20 institutions contributing to and analyzing the model [*Rotman et al.*, this issue].

2.2. GMI Model Description

The GMI model is a global, 3-D chemistry-transport model (CTM) containing a complete prognostic stratosphere with parameterizations to represent tropospheric and surface loss processes. A complete description of the GMI model is presented by *Rotman et al.* [this issue]; the following is a condensed summary [see also *Kawa et al.*, 1999, Appendix G].

The "best" meteorological fields selected for this assessment [see *Douglass et al.*, 1999] are obtained from a simulated year of the Middle Atmospheric Version of the National Center for Atmospheric Research (NCAR) Community Climate Model, Version 2 (CCM2) (MACCM2) GCM [*Boville*, 1995]. The top of the model is 0.025 hPa (approximately 75 km) with fields provided on 44 vertical levels. The horizontal resolution is approximately 4° latitude and 5° longitude. Advection in all three directions uses a variable-order multidimensional flux form of the semi-Lagrangian method, an up stream-biased monotonic grid point scheme [*Lin and Rood*, 1996]. The choice of this scheme was made after comparison of tracer simulations with different advection schemes [*Kawa et al.*, 1999; *Rotman et al.*, this issue]. In addition, this version of MACCM2 included an extra gravity wave parameterization that improved the temperatures in the Antarctic polar vortex, however, at the same time, yielded Arctic temperatures, which were too high compared to observations [*Douglass et al.*, 1999].

The photochemistry within the GMI model is solved using the semi-implicit scheme of *Ramaroson* [1989]. Reactions in the stratospheric mechanism include those comprising the families O_x, NO_y, ClO_y, HO_y, BrO_y, and CH_4 and its oxidation products (46 transported species, 116 thermal reactions, and 38 photolytic reactions). Photolysis rates are obtained from a clear-sky lookup table developed by S. R. Kawa, where normalized radiative fluxes are a function of cross section (which is in turn a function of temperature, species, and wavelength), pressure, solar zenith angle, and column ozone. Temperature-dependent cross sections, quantum yields [*DeMore et al.*, 1997], and solar fluxes are tabulated separately.

The GMI polar stratospheric cloud (PSC) parameterization calculates surface area densities for both Type 1 and Type 2 PSCs [*Considine et al.*, 2000]. The parameterization assumes Type 1 PSCs to be supercooled ternary liquid droplets (STS) and Type 2 PSCs to be water ice. When a Type 2 PSC forms, the HNO_3 contained within the STS aerosol is converted to nitric acid trihydrate (NAT). The HNO_3 abundance contained within the NAT aerosol is assumed to deposit on the ice aerosol. Both Type 1 and Type 2 PSCs sediment in the GMI PSC parameterization, resulting in irreversible dehydration and denitrification of the polar vortex.

The most appropriate way to include water in the model for the HSCT impact assessment would have been to carry out a simulation for the MACCM2 for 2015 conditions, after having thoroughly compared present-day simulations of this version with available lower-stratospheric data. Alternatively, the model could have been forced at the hydropause with a "reasonable" boundary condition for H_2O, again appropriate for 2015 conditions. Given the time constraints of the required assessment, we adopted the following approach to provide a reasonable representation of stratospheric water. The GMI model uses a monthly zonal mean background H_2O distribution derived from the Goddard Space Flight Center (GSFC) 2-D model [*Jackman et al.*, 1996]. The GSFC 2-D model was integrated with 2015 CH_4 boundary condition to derive the additional H_2O from CH_4 oxidation (see section 3.1). This additional CH_4 oxidation component of stratospheric H_2O was approximately 1-2% near the tropopause and 8% in the mesosphere relative to 1990 conditions. Because it is necessary to predict PSC occurrence and dehydration in a model designed to assess the effects of HSCTs, dehydration processes were not included in the GSFC 2-D integration.

2.3. GMI Model Evaluation

A methodology for semiobjective evaluation of the performance of different meteorological fields within the GMI model has been described by *Douglass et al.* [1999]. That methodology utilized simulations of N_2O, CO_2, and a seasonal tracer, in combination with a comparison of the GCM temperatures to existing climatologies. The simulations utilized off-line production and losses, when needed. A grading scale was assigned to each parameter, with the consensus of the GMI Science Team. Since there are no a priori reasons to give more weight to a specific set of simulations, they were all weighted equally. This "grading" provided an important tool for initial evaluation of a given set of fields by tracer simulations, before performing intensive calculations with full chemistry. The grading was applied to the meteorological fields from the MACCM2, as well as to 1 year from the GEOS-Stratospheric Tracers of Atmospheric Transport (STRAT) simulation from the NASA/Goddard Data Assimilation Office (DAO), and to a 1 year simulation from the Goddard Institute for Space Studies (GISS) GCM, version II. *Douglass et al.* [1999] indicated that the MACCM2 fields performed better overall than the other fields. This set of winds was thus chosen for the assessment calculations. It must be emphasized, however, that none of the meteorological fields provided a very good representation of all the processes. The adopted version of MACCM2 meteorological fields, in particular, also exhibited a very warm Arctic vortex, which precluded a good simulation of PSC processes. Thus the development and use of better meteorological fields is a necessity for future assessments.

The GMI model with the MACCM2 winds underwent a further series of comparisons of the full-chemistry results with other observations [*Park et al.*, 1999; *Kawa et al.*, 1999]. These comparisons utilized calculations carried out for 1996 conditions of chlorine and bromine loading, source gas concentrations, and aerosol loading. Tracer correlations were examined in more detail. Overall, the model reproduced the correlation of NO_y with N_2O observed in the lower stratosphere. However, the scatterplot of NO_y versus N_2O calculated by the model fell below that derived from Atmospheric Trace Molecule Spectroscopy Experiment (ATMOS) data near the midstratospheric peak; the calculated concentrations of NO_y in the lower stratosphere are smaller than those observed by the ER2, and the mean age of air is younger than that derived from observations, as found in most other models [*Park et al.*, 1999]. Comparisons were also carried out for ozone profiles with an ozone sonde climatology [*Logan*, 1999]. Model results are in very good agreement with observations, particularly in the lower stratosphere, where many two-dimensional models tend to overestimate the ozone concentrations [*Park et al.*, 1999]. The ozone columns are in reasonable agreement with satellite data, and the model does produce an Antarctic ozone hole, although not as deep as observations for

some of the recent years due to differences in temperature and a somewhat weak downwelling within the modeled Antarctic vortex. We must emphasize that the above agreements/disagreements with data are not independent; that is, it is not clear that if we "fixed" the model to agree better with the NO_y observations, we would necessarily preserve the current agreement with ozone. Thus the GMI model faces the same challenge as other simulations of the atmosphere, that is, improvement in the overall performance of the model, which requires improving the agreement with certain observations while maintaining the achieved consistency with others.

Two areas of discrepancy with observations were identified in the HSRP Assessment Report [*Kawa et al.*, 1999] as having important implications for the results presented here: (1) The model mean age of air is young (by 1-2 years) compared to those derived from CO_2 and SF_6 observations [*Park et al.*, 1999; *Kawa et al.*, 1999; *Hall et al.*, 1999]. Although it is not clear what the quantitative relationship is between mean age of air and exhaust accumulation calculated by different models [*Kawa et al.*, 1999; *Hall and Waugh*, 2000], this discrepancy indicates that the model is likely to underestimate the aircraft exhaust accumulation. (2) Although there is good agreement between the calculated and observed correlations of NO_y versus N_2O in the lower stratosphere, the model underestimates the concentrations of NO_y (and overestimates the concentrations of N_2O) in this region. This is also a problem with other 3-D models [*Kawa et al.*, 1999]. Model analysis (see below) indicates that, for low levels of background NO_y, addition of aircraft NO_y in the 18-20 km region results in a net increase in ozone, due to the coupling of NO_x with other ozone catalytic cycles described by *Wennberg et al.* [1994]. The low background NO_y in the GMI model translates into a calculated large positive column ozone change due to HSCT emissions over most of the globe. The reason for the NO_y discrepancy needs to be ascertained to improve the future assessment results for this and other models.

The chemical mechanism used in the GMI 3-D model was evaluated within a photostationary state box model. This evaluation tests two aspects of the chemistry. First, the chemical mechanism in the GMI model is similar to that used in the photostationary state box model tested by comparison with observations from aircraft, balloon- and space-borne platforms by R. Salawitch [see, e.g., *World Meteorological Organization* (WMO), 1999, chapter 5]. In particular, the chemical partitioning in a substantial number of observations can be reproduced with the assumption of diurnal steady state. This can be interpreted as saying that stratospheric motions are such that radical partitioning is in diurnal steady state, provided that we use the right chemical mechanism. Thus the appropriateness of the GMI chemical mechanism has already been tested in the Salawitch comparisons with observations. Second, the reservoir gas concentrations derived from a present-day GMI 3-D model integration were adopted as constraints to the photostationary state box model [see *Park et al.*, 1999; R. J. Salawitch, personal communication, 2000] and radical distributions were derived. These radical abundances were then compared to the radicals derived in the GMI 3-D model. The calculations from the GMI assessment model are within 10 to 15% of those produced by the constrained photostationary model [*Kawa et al.*, 1999]. This agreement indicates the following: (1) The numerical scheme for solving the chemistry is reasonably accurate. (2) The stratospheric motions in the model are such that the radical partitioning is in diurnal steady state (as seems to be the case for the real atmosphere). In addition, the numerical scheme was specifically validated by comparison to a Gear numerical solution approach [*Kawa et al.*, 1999, Appendix E]. Results from this comparison showed the Ramaroson [1989] numerical solution approach to be very accurate.

Table 1. Source Gas Boundary Conditions for the 2015 Atmosphere [*Stolarski et al.*, 1995]

Species	Units	Year 2015
CFC-11	pptv	220
CFC-12	pptv	470
CFC-113	pptv	80
CCl_4	pptv	70
HCFC-22	pptv	250
CH_3CCl_3	pptv	3
HCFC-141b	pptv	12
Halon-1301	pptv	1.4
Halon-1211	pptv	1.1
CH_3Cl	pptv	600
CH_3Br	pptv	10
CH_4	ppbv	2052
N_2O	ppbv	333

3. HSCT Assessment Scenario

3.1. Source Gas Boundary Conditions and Aerosol Surface Area Density

The source gas lower boundary conditions (e.g., N_2O, CH_4, CFCs, HCFCs, and halons) were set and held at constant mole fractions for the duration of the model integrations (i.e., surface fluxes were not assumed). These boundary conditions are shown in Table 1. The halogen source gases for 2015 were taken from *Stolarski et al.* [1995]. Source gases CH_4 and N_2O were taken from the IS92a scenario given by *IPCC* [1996; Tables 2.5a and 2.5b]. CH_3Br was taken from the IS92a scenario given by *IPCC* [1996; Table 2.2]. Surface boundary conditions for the organic chlorine and bromine species were specified such that at the top of the stratosphere, the total inorganic chlorine (i.e., Cl, ClO, Cl_2, OClO, $2Cl_2O_2$, HOCl, HCl, $ClONO_2$, BrCl) and inorganic bromine (i.e., Br, BrO, HBr, HOBr, $BrONO_2$, BrCl) were 3.0 parts per billion by volume (ppbv) and 12.5 parts per trillion by volume (pptv) respectively.

The surface area density (SAD) for sulfate aerosols in the background atmosphere was specified according to *WMO* [1992; Table 8-8], which represents the 1979 SAD as determined by data taken with the Stratosphere Aerosol and Gas Experiment (SAGE) instrument on the NIMBUS 7 satellite. This sulfate SAD is representative of a volcanically clean atmosphere. In the present study there was no attempt to examine the sensitivity of results to increases in SAD during volcanically active periods. In addition, this study did not examine the impact of increased SAD from sulfur oxidation in the HSCT fuel. Both of these SAD sensitivities were examined and discussed using 2-D models in recent assessment reports [*Kawa et al.*, 1999; *IPCC*, 1999].

3.2. Description of HSCT Fleet Scenario

The HSCT fleet considered in this paper is based on a conceptual design for a Mach 2.4 supersonic transport cruising supersonically at 17-20 km altitude. The aircraft would be expected to be used primarily on long intercontinental routes with supersonic flight only over water to avoid sonic booms over populated areas. Since detailed industry forecasts do not extend

more than 20 years into the future, the detailed projections of air traffic for the year 2015 have been used in order to explicitly account for changes in subsonic technology and displacement of subsonic air traffic by the HSCTs. Although the number of HSCTs is not expected to reach 500 until after 2015, 2-D model calculations have shown that the calculated HSCT ozone impact would not be very sensitive to decreases in ambient stratospheric chlorine abundance expected after 2015 [*Stolarski et. al.*, 1995; *Kawa et al.*, 1999; *IPCC*, 1999].

The baseline comparison for these calculations is an all-subsonic aircraft fleet projected to the year 2015 and including both scheduled [*Baughcum et al.*, 1998] and unscheduled air traffic. The latter includes military, charter, and general aviation [*Mortlock and Van Alstyne*, 1998]. The HSCT scenario is based on a NASA technology concept airplane (TCA) and assumes a fleet of 500 supersonic aircraft with a corresponding displacement of subsonic traffic by the supersonic fleet [*Baughcum and Henderson*, 1995, 1998]. For the calculations presented here, the NASA combustor goal of a NO_x emission index (EI NO_x) of 5 grams (as NO_2)/kilogram fuel burned is assumed for supersonic cruise. The emission index for H_2O is also proportional to the amount of HSCT fuel consumed. Here a value of 1237 grams (as H_2O)/kilogram fuel burned was assumed for this calculation. These scenarios were also used in the recent IPCC special report [*IPCC*, 1999] and the NASA HSRP/AEAP assessment [*Kawa et al.*, 1999].

The geographical distribution of the assumed HSCT emission scenario is shown in Plate 1. The peak stratospheric emissions occur at northern midlatitudes in the 17-20 km altitude band. For this scenario, 6.5×10^5 kg/d of NO_x and 1.6×10^8 kg/d of water vapor are emitted at altitudes above 17 km. A more detailed description of this scenario is given by *Baughcum and Henderson* [1998].

The GMI 3-D model was integrated for 6 years (from a common 2015 atmosphere initial condition) for both the subsonic only scenario and the HSCT plus subsonic scenario (regarded in this study as the base scenario). We found this integration length was sufficient since the difference in constituent concentrations between years 5 and 6 were of the order of a few percent.

4. HSCT Assessment Results

This section summarizes the calculated changes in NO_y and H_2O and the consequent change in local and column ozone due to HSCT emissions. The enhanced NO_y and H_2O distribution is critically dependent on the tendency of the GMI model's transport. As mentioned above, this version of the GMI model uses meteorological fields from the NCAR Middle Atmosphere Community Climate Model [*Boville*, 1995]. Evaluation of the transport is briefly discussed in section 5.1 and in detail by *Douglass et al.* [1999], *Park et al.* [1999], and *Rotman et al.* [this issue]. The HSCT-enhanced H_2O and NO_y changes the relative abundances of inorganic nitrogen oxides (NO_x), hydrogen oxides (HO_x), chlorine oxides (ClO_x), and bromine oxides (BrO_x) in the lower stratosphere, modifying the ozone loss characteristics of this region and therefore changing local ozone abundance.

4.1. Change in NO_y and H_2O From HSCT Fleet

The HSCT-induced change in zonal mean NO_y, defined here as delta-NO_y, is shown in Figure 1a. The GMI model calculates a maximum increase of approximately 0.6-0.7 ppbv in the lower stratosphere somewhat poleward from the latitude of peak emission in the NASA emission scenario, but at a similar altitude (see Plate 1). Most of the delta-NO_y is confined to the Northern Hemisphere, lower stratosphere; however, a delta-NO_y of approximately 0.2 ppbv is calculated at 30°S. In addition, a significant amount of HSCT-derived NO_y is transported to the middle stratosphere. For example, in June, a delta-NO_y equal to 0.1 ppbv is calculated at 40 km.

In Figure 1b, the HSCT-induced change in H_2O, defined here as delta-H_2O, is shown for the month of June. The contour distribution is similar to that of delta-NO_y, except in the upper stratosphere (i.e., above 30 km), where the delta-H_2O magnitudes do not fall off as rapidly. This is due to the fact that, unlike NO_y, H_2O does not have a significant chemical sink in the middle and upper stratosphere.

In winter the adopted meteorological fields yield a fairly isolated region within the Northern Hemisphere polar vortex (see Plate 2). For example, a sizable barrier to transport can be deduced on the 500 K potential temperature surface (approximately 20 km altitude) from the delta-NO_y results. Calculated delta-NO_y values poleward of 60°N are up to a factor of 2 less than that outside this region. This is not seen in two-dimensional model HSCT studies [*Kawa et al.*, 1999]. The fact that this barrier to transport and smaller changes in NO_y (and H_2O) within the polar vortex is seen in the three-dimensional calculation but not in two-dimensional calculations suggests that 2-D model estimates of the change in PSC surface area resulting from the general increase in lower stratospheric NO_y and H_2O may be excessive. We do not attempt quantitative evaluation of this effect because of the warm bias in our modeled Northern Hemisphere lower stratospheric temperatures. See section 5.4 for more discussion on the potential for HSCT-induced change in polar processes.

4.2. Change in Ozone From HSCT Fleet

The calculated changes in local and column densities of ozone due to HSCT emissions are shown in Figures 2a and 2b, respectively. The local change in ozone is consistently negative above approximately 22-25 km (depending on the latitude). The maximum decrease in ozone is approximately 40-50 ppbv between 30 and 40 km, decreasing in magnitude with increased altitude above this level. Below 22-25 km, the HSCT-induced ozone change is positive, maximizing at approximately 20 ppbv around 20 km, and decreasing in magnitude toward the tropopause. It should be noted that the GMI 3-D model does not include a realistic representation of tropospheric chemical and physical processes; therefore the tropospheric ozone change has been removed from all results shown in this study. This was done by assuming that the tropopause was defined by the 200 ppbv ozone mole fraction contour. Everything below this ozone value was assumed to be in the troposphere (see shaded region in Figure 2a). This approach has only a minor impact on the HSCT-induced column ozone change (Figure 2b).

The change in column ozone shown in Figure 2b is a few tenths of a percent positive everywhere, except during the spring season at high latitudes in the Southern Hemisphere. In the Northern Hemisphere the calculated percent change in column ozone shows little seasonal structure. The percent change in column ozone is fairly constant between 30°N and 30°S. The GMI model yields changes of +0.2%, and +0.05% in Northern and Southern Hemisphere total column ozone, respectively. The *IPCC* [1999] quoted a central value of –0.8% and –0.3% in Northern and Southern Hemisphere total column ozone, respectively; this value

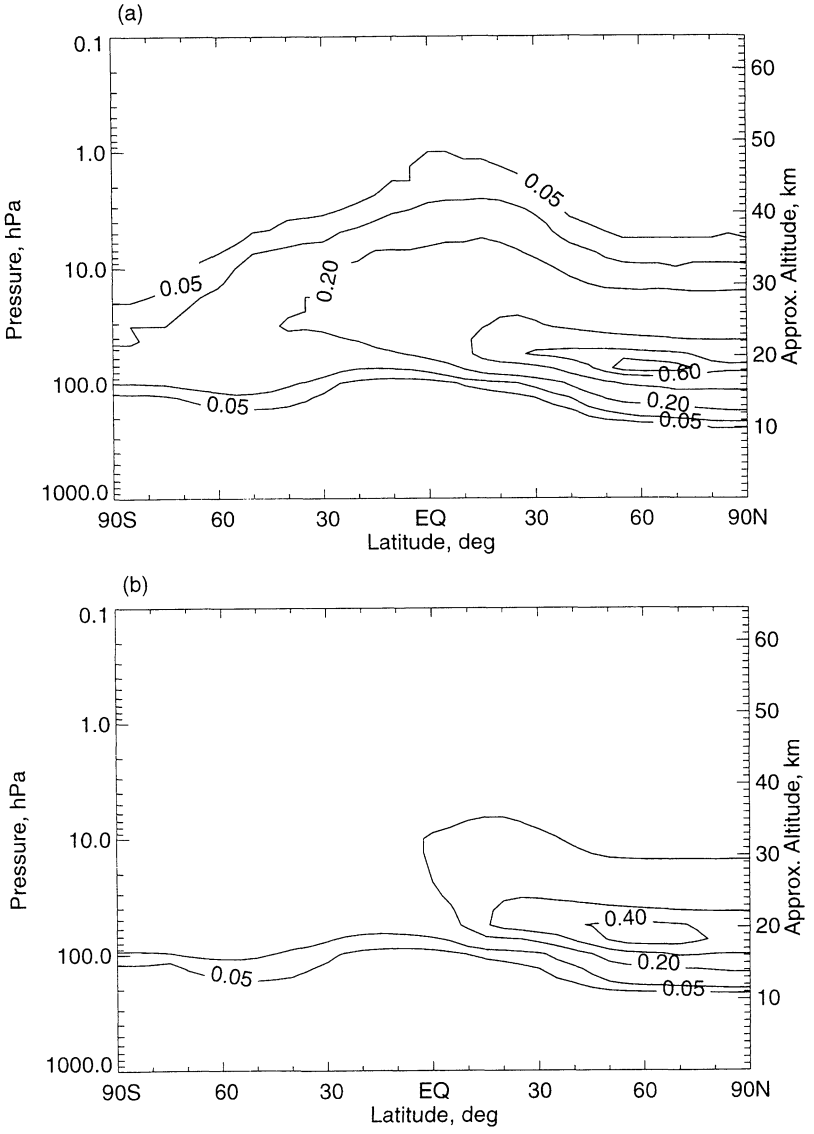

Figure 1. Calculated HSCT-induced change in (a) NO_y and (b) delta-H_2O during June. Both delta-NO_y and delta-H_2O are the difference between a "HSCT plus subsonic" assessment calculation and a "subsonic only" calculation. Contour lines are 0.05, 0.1, 0.2, 0.4, and 0.6 ppbv for delta-NO_y and 0.05, 0.1, 0.2, 0.3, 0.4 ppmv for delta-H_2O.

was obtained from the atmospheric and environmental research (AER) 2-D model, since the results of this model seemed to be midway between the highest and lowest results. The HSRP report [*Kawa et al.*, 1999] carried out a more complete analysis of model results in the context of their agreement with atmospheric measurements. On the basis of this analysis they estimated a central value of -0.4% in the Northern Hemisphere. They also quoted a Northern Hemisphere probable range of –2.5% to +0.5%. It should be noted that both the IPCC and HSRP reports included the assumption of 10% sulfate gas-to-particle conversion in the aircraft plume.

The contribution of different altitude regimes to the total change in column ozone is illustrated in Figure 3. In Figure 3a the change in column ozone (in Dobson units (DU)) is plotted for altitudes between 25 and 60 km. The contribution from this region is negative everywhere with values ranging between –0.4 and –0.8 DU. This is in striking contrast to the positive total column ozone percentage changes shown in Figure 2b. In addition, the negative change at high latitudes in the Southern Hemisphere as shown in Figure 2b is not particularly pronounced above 25 km in Figure 3, indicating that the net negative change in ozone is contributed by the region below 25 km, where PSC processes are important. The contribution from the tropopause (defined as the ozone 200 ppbv level) to 25 km range (Figure 3b) is positive everywhere, except, as noted above, during the Southern Hemisphere spring period. In the mid- to- high latitudes, Northern Hemisphere, integrating between the tropopause and 25 km gives up to a +1.6 DU change; adding to this, the negative change above 25 km of approximately –0.4 DU gives the resultant positive change of +1.2 DU for the entire column. Therefore the overall Northern Hemisphere column ozone change is mostly determined by the positive change below 25 km. The reason these altitude regions show dramatically different sensitivities to HSCT-induced NO_y and H_2O change will be discussed in section 5.

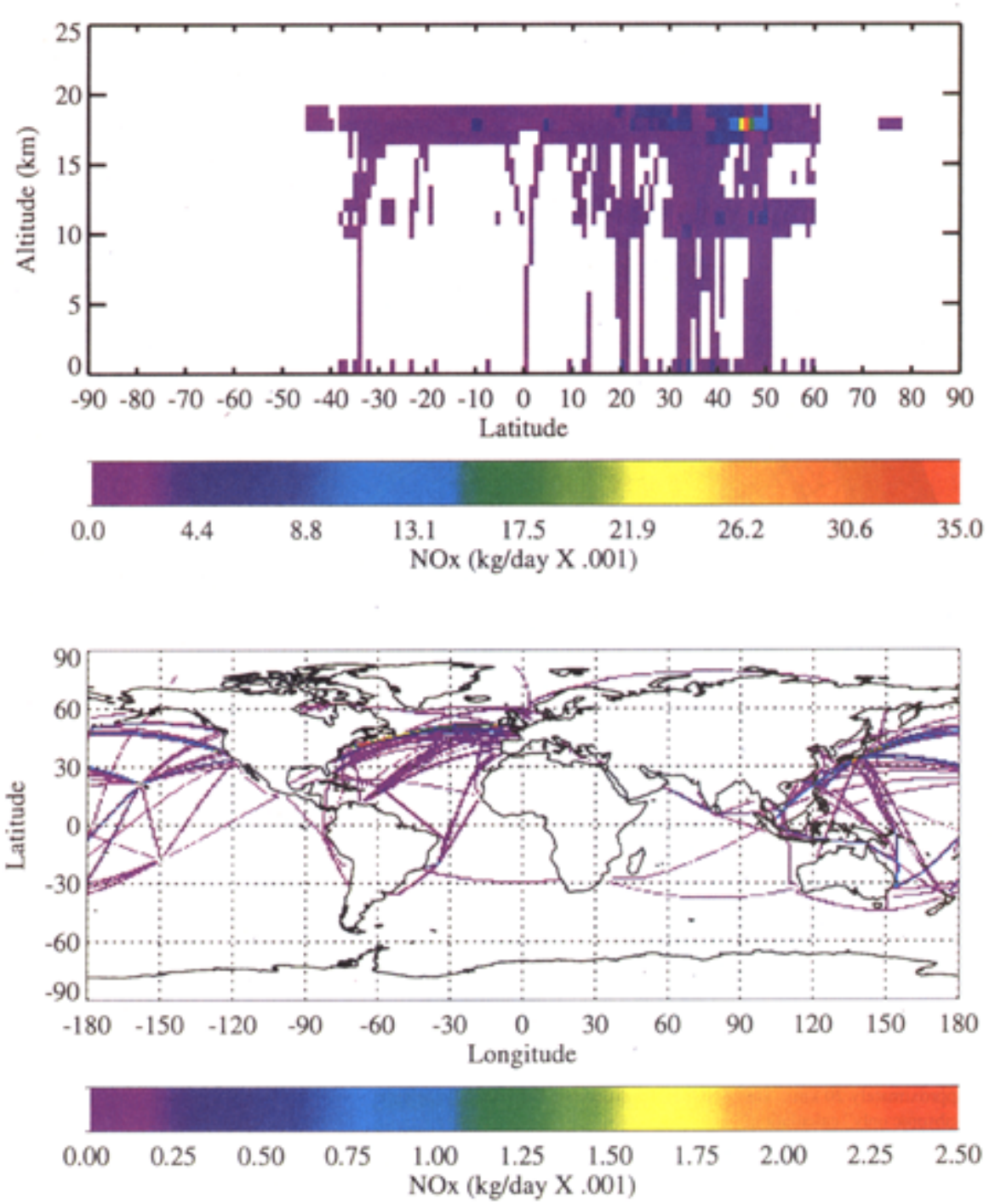

Plate 1. NASA HSCT 2015 NO_x emission scenario (500 aircraft) used in this assessment. (top) Annual zonal-average emission of NO_x (as NO_2 kg/d per 1°latitude x 1-km altitude grid cell) from HSCTs. (bottom) Column-integrated NO_x (as NO_2 kg/d per 1° longitude x 1° latitude grid cell) from HSCTs.

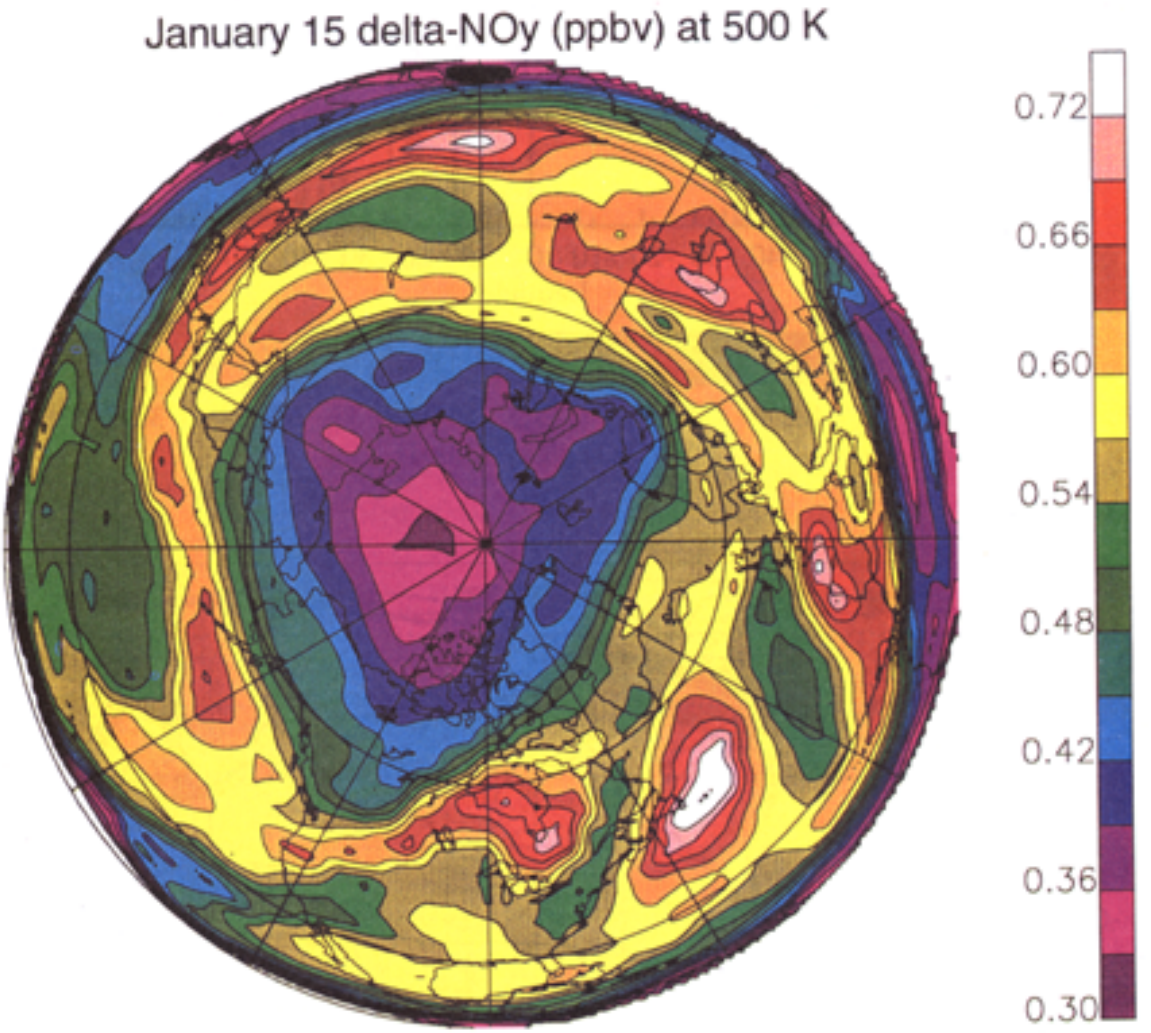

Plate 2. Calculated HSCT-induced change in NO_y (ppbv) on the 500 K potential temperature surface on January 15 (approximately 20 km). Delta-NO_y is the difference between a "HSCT plus subsonic" assessment calculation and a "subsonic only" calculation.

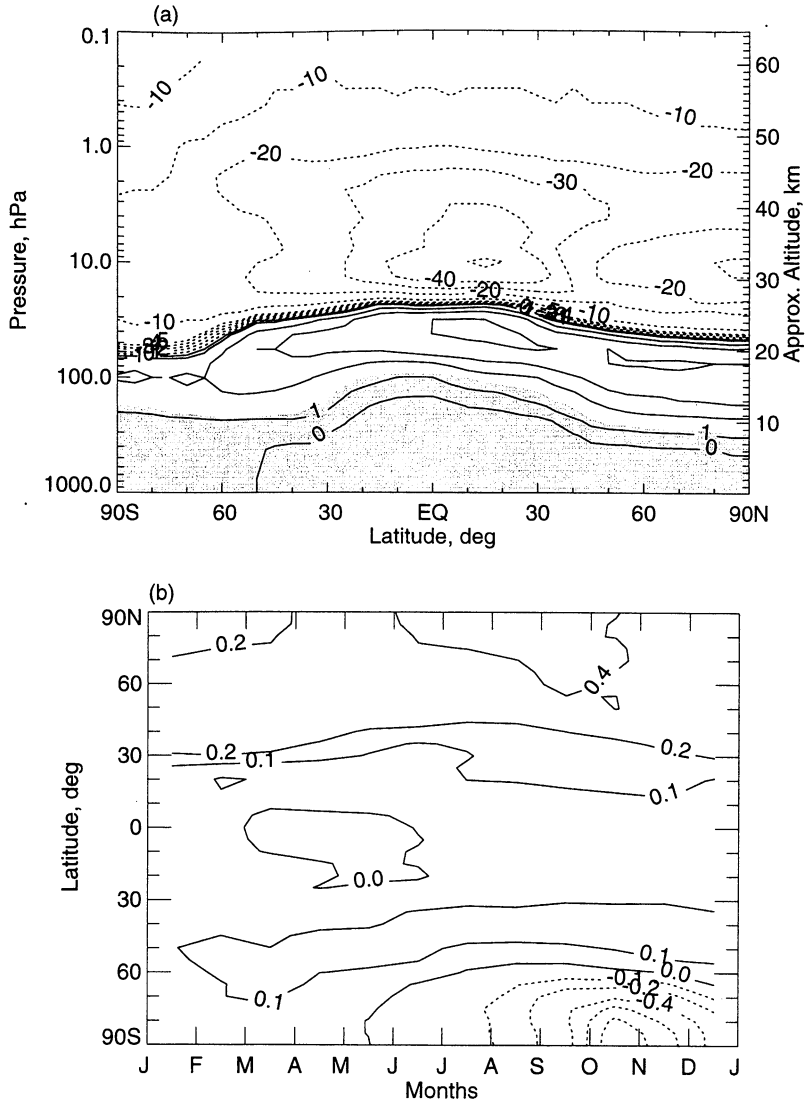

Figure 2. Calculated HSCT-induced change in (a) local O_3 mixing ratios (ppbv) during June and in (b) total O_3 column density (%). Delta-O_3 and delta-column O_3 are differences between a "HSCT plus subsonic" assessment calculation and a "subsonic only" calculation. Contour lines are ± 0, 5, 10, 20, 30, 40 ppbv for local delta-O_3 and ± 0, 0.1, 0.2, 0.4, 0.6, 0.8 % for delta-column O_3.

5. Interpretation of Assessment Results

The HSCT Assessment Report [*Kawa et al.*, 1999] identified the model-calculated mean age of air and NO_y concentrations in the lower stratosphere as crucial diagnostics of model performance. This section will discuss the performance of the GMI model with respect to the above diagnostics, and analyze the impact of the discrepancies. In addition, we illustrate how additional discrepancies between calculated and observed ozone and water could contribute as much as the above diagnostics to potential biases in the results of assessment models [*Douglass et al.*, 1999].

This section is divided into four parts. Section 5.1 discusses the use of observations to gauge the accuracy and biases of calculated perturbations to NO_y and H_2O due to aircraft emissions. Section 5.2 evaluates the concentrations of ambient (unperturbed) N_2O, NO_y, and O_3 calculated by the GMI model, and highlights the importance of accurately representing these key species. Section 5.3 discusses the derived local ozone change and how this relates to ozone loss processes in the GMI 3-D and Lawrence Livermore National Laboratory (LLNL) 2-D models. Note, in this study, "ozone loss" is synchronous with "odd-oxygen loss" (defined as $O_3+O^3P+O^1D$). Finally, the impact of HSCT-induced H_2O and NO_y perturbations on polar heterogeneous chemical processes is discussed in section 5.4

5.1. HSCT-Induced Delta-NO_y and H_2O Abundances

The calculated impact of HSCTs on stratospheric ozone is directly related to a model's calculated accumulation of HSCT-derived NO_y and H_2O. Since these predicted accumulations cannot be tested directly with observations, it is important to

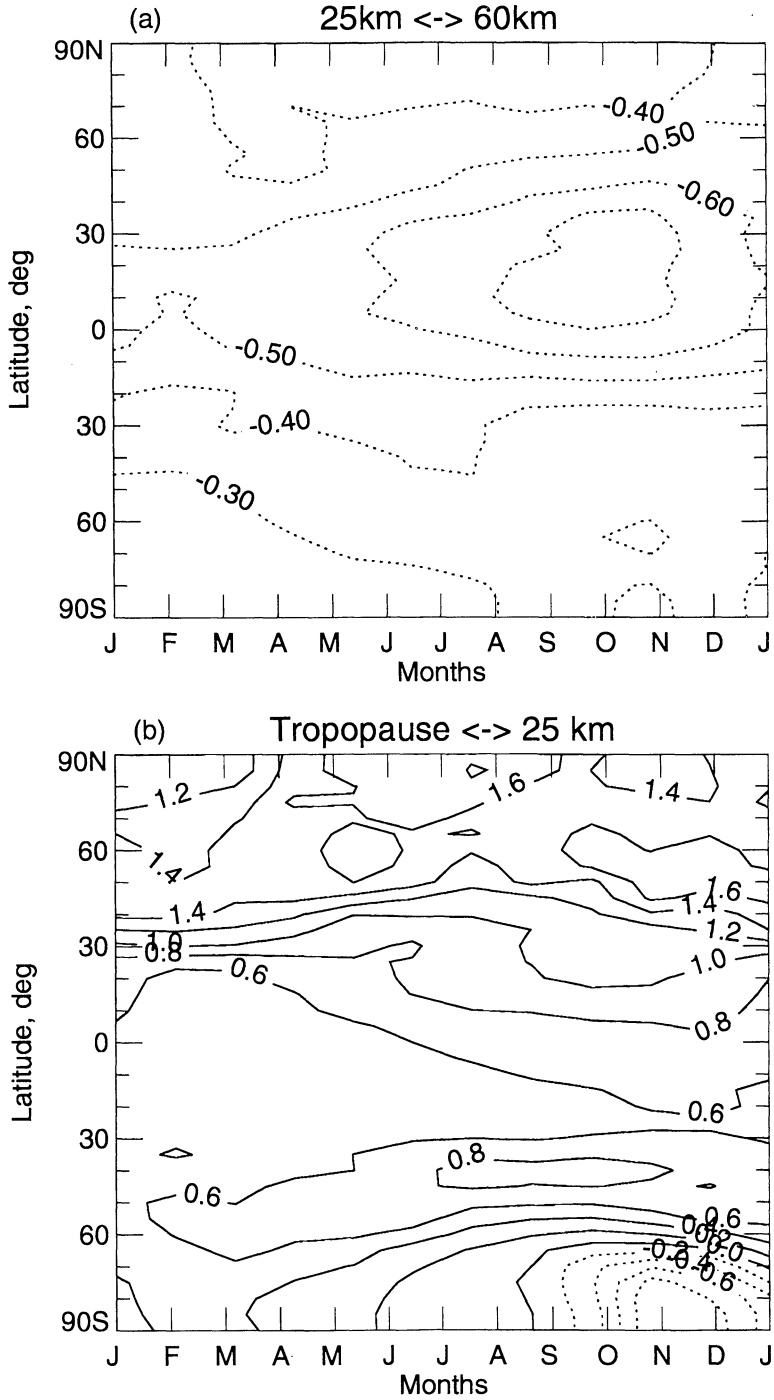

Figure 3. Calculated HSCT-induced change in total column O_3 density (Dobson units) (a) between 25–60 km and (b) the tropopause to 25 km (see text for details on the tropopause definition).

identify suitable observational diagnostics which can be directly related to the quality of the calculated accumulations. We expect a positive correlation between the mean age of air derived from CO_2 and SF_6, and stratospheric residence time [*Boering et al.*, 1996]. However, as discussed by *Kawa* [1999], it is not yet possible to quantify the relationship between residence time of aircraft exhaust emissions and the mean age of air. In particular, the relationship between mean age of air and accumulation seems to be different between 2-D and 3-D models, with accumulation in 3-D models being less sensitive to mean age of air [*Park et al.*, 1999; *Kawa et al.*, 1999]. In addition, it should be noted that the mean age of air is derived for an infinite-life tracer injected at the tropical tropopause, not a tracer like aircraft NO_y that is injected into the lower stratosphere and has loss processes at the top of the stratosphere.

Keeping the above caveats in mind, it is reasonable to think that if a model underestimates the observed mean age of air, it could also underestimate the burden of HSCT-induced NO_y and H_2O. In Figure 4 an altitude versus latitude contour plot is shown for the annual-mean age of air derived from observations (Figure

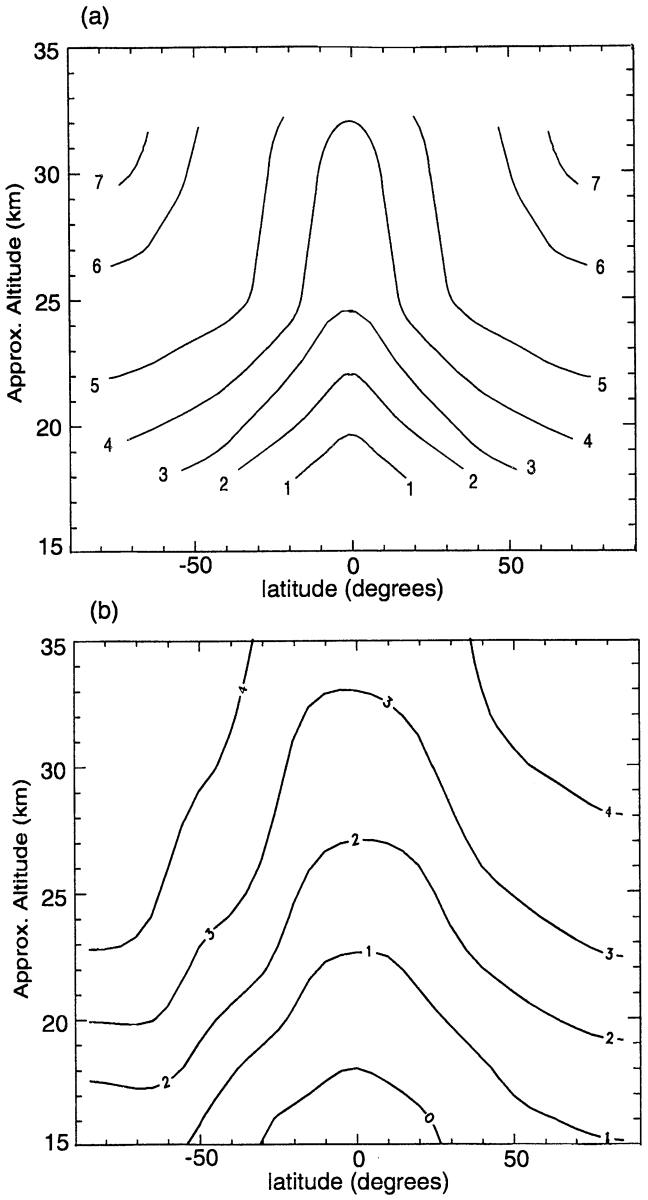

Figure 4. (a) Comparison of annual-averaged zonal-mean age of air derived from observations. Figure 4a is a schematic based on estimates of age of air taken from aircraft and balloon measurements of CO_2 and SF_6 (see *Park et al.* [1999] for details). Note that as the data are primarily from the Northern Hemisphere, the schematic is hemispherically symmetric. (b) Age of air calculated from the GMI 3-D model.

4a) and GMI model-derived (Figure 4b) annual-mean age of air. This figure is modified from the NASA Model and Measurement II Workshop Report [*Park et al.*, 1999]. In general, the GMI model underestimates the mean age of air. For example, in the equatorial region near 25 km, the GMI model underestimates the mean age of air by 1.5 years. In the polar regions near 30 km the GMI model underestimates the mean age of air by 2-3 years. This would also suggest that the model underestimates the HSCT-induced NO_y and H_2O stratospheric burdens. However, it does not follow that the accumulation is underestimated by the same factor as is the mean age of air. Additional research is needed to better quantify how sensitive the mean age of air diagnostic is in evaluating the HSCT-induced NO_y and H_2O burden [*Hall and Waugh*, 2000]. Thus, at present, it is not possible to evaluate quantitatively the magnitude of the bias in calculated accumulations due to the discrepancy in mean age of air.

5.2. Impact of Errors in Ambient Atmosphere on HSCT Perturbation

Figure 5 shows a comparison of the GMI model to N_2O, NO_y [*Strahan et al.*, 1999, also manuscript in preparation, 2000], and O_3 summertime [*Logan*, 1999], midlatitude climatologies. This is a subset of the model/data comparison shown by *Park et al.* [1999] and *Kawa et al.* [1999]. At mid-latitudes, vertical profiles of N_2O, NO_y, and O_3 are determined by a combination of stratosphere-troposphere exchange, downwelling residual circulation, diffusive mixing from wave breaking, and chemical production and loss. The overall contributions to the N_2O, NO_y, and O_3 vertical profiles from these individual processes are difficult to isolate. In the lower stratosphere at midlatitudes the GMI model tends to overestimate the N_2O abundance and underestimate the NO_y abundance. This would suggest that the model transport is in error.

The model/data comparison for ozone is in much better agreement. Here the GMI model slightly underestimates the ozone abundance in the lower stratosphere (below 25 km). Above 25 km the model is slightly greater than the *Logan* [1999] ozone climatology. This result is somewhat in contrast to the N_2O figure, essentially highlighting the complexity of the transport/chemistry coupling. In the troposphere (below approximately 10-12 km) the GMI model greatly underestimates the ozone abundance. As mentioned above, this is expected since the GMI model does not represent emission sources (i.e., lightning, aircraft, surface convection) that would contribute to in situ net ozone production (i.e., from hydrocarbon-NO_x-HO_x chemistry [*Crutzen*, 1973]).

The impact of possible systematic errors in the background chemical state of the model stratosphere was examined with a series of sensitivity tests. Selecting typical midlatitude conditions from the GMI CTM, we used a photochemical box model to calculate the local net chemical tendency of ozone, dO_3/dt, both for the background atmosphere and for one with a 10% increase in NO_y, typical of an HSCT perturbation. The difference between these two tendencies, Delta(dO_3/dt), is shown in Figure 6 (solid line) for the standard GMI simulation, July 15, 42°N latitude and 0° longitude. At each altitude the instantaneous species distributions (and SADs) from the 3-D model were integrated beginning at local midnight for 2 days (without transport), and the 24-hour average net chemical tendency for O_3 was reported for the second day. The deviation of this altitude profile of Delta(dO_3/dt) from zero demonstrates how an NO_y increase would drive a change in ozone. In the lower stratosphere, ozone is controlled also by transport, and the actual change in O_3 would involve an average of these Delta(dO_3/dt) values over a range of altitudes, latitudes, and longitudes that are connected through transport. This midlatitude change in dO_3/dt is still a good measure, or proxy, of the perturbation to O_3 calculated for the HSCT scenario with the 3-D model: Delta(dO_3/dt) increases over most of the lower stratosphere, with decreases above 24 km where NO_y catalytic loss is more important; compare Figures 6, 7, and 9.

It is now easy to examine how the modeled HSCT perturbations may be affected by systematic errors in the simulation of the background atmosphere. The same box model calculations were repeated once for a 50% increase in each of the ambient profiles of NO_y, O_3, and H_2O (in both perturbed and

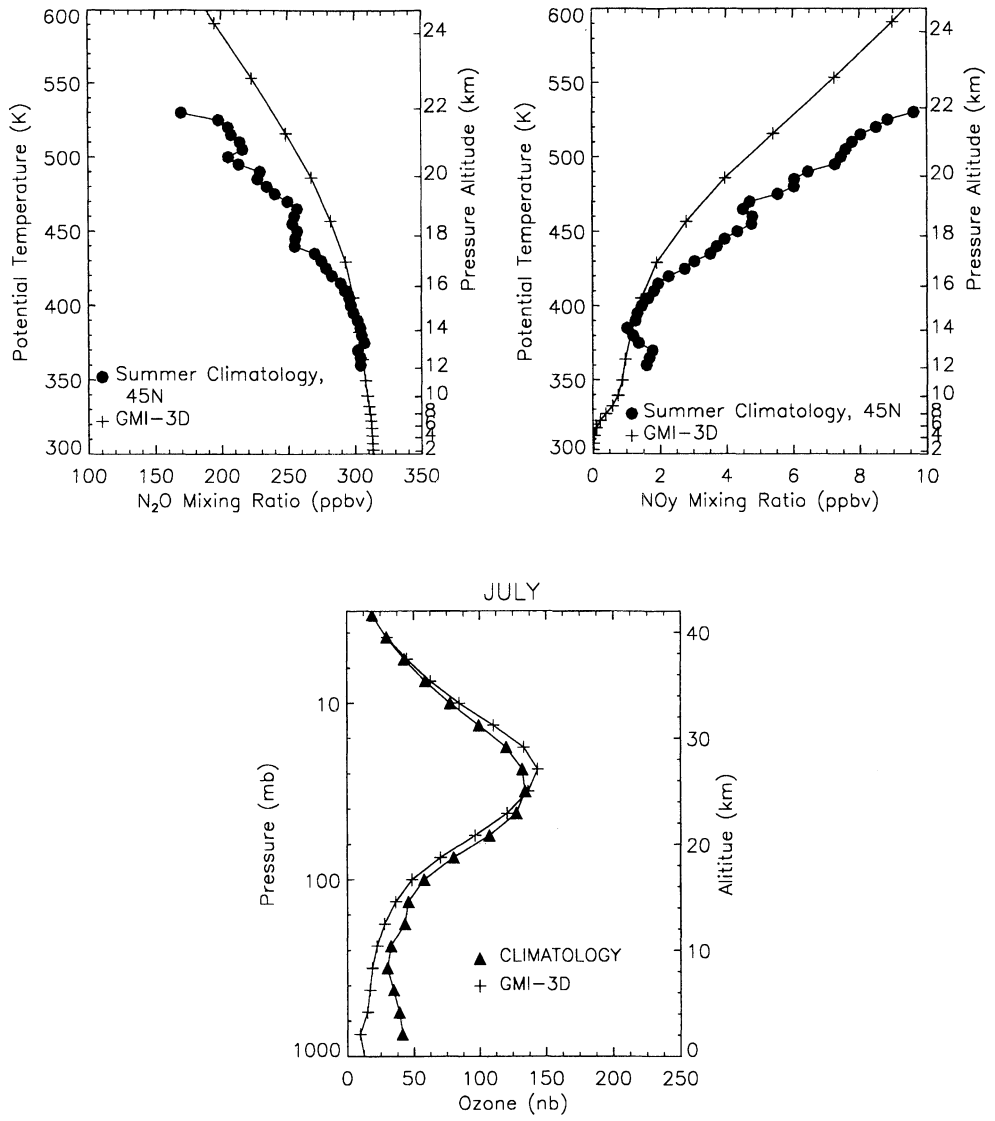

Figure 5. Model/data comparison for N_2O, NO_y, and ozone. See text for details.

reference scenarios). These offsets were selected since, for example, the GMI model systematically underestimates NO_y in the lower stratosphere (see Figure 5). At 50% higher ambient NO_y (dash-dot-dash line in Figure 6) the change in ozone tendency for the +10% NO_y perturbation is more negative throughout the lower stratosphere, and Delta(dO_3/dt) turns negative by 22 km. Thus at greater concentrations of NO_y, its catalytic cycle dominates ozone loss, and further increases lead to additional depletion [*Wennberg et al.*, 1994]. At 50% higher ambient H_2O abundance (dash-dot-dot-dot line), Delta(dO_3/dt) in the lower stratosphere is also more positive, as in the case with higher ambient O_3, but the crossover point is 1 km higher. The greater HO_x concentrations in the ambient atmosphere in the raised H_2O case mean that addition of NO_y reduces ozone catalytic loss that is dominated by the HO_x cycle, consistent with current measurements and modeling of O_3 loss in the lowermost stratosphere [*Wennberg et al.*, 1994; *Salawitch et al.* 1994]. With 50% higher ambient O_3 levels (dashed line) the ozone response to the NO_y perturbation is more positive, about 30% greater below 24 km, although the altitude of crossover to negative values is almost unchanged from the reference simulation. Higher ambient O_3 tends to lower the NO_x/NO_y ratio and thus increase the ClO_x/Cl_Y ratio [*Kawa et al.*, 1999; *Douglass and Kawa*, 1999]. Increasing inorganic ClO_x radicals relative to NO_x radicals tends to give a more positive (or less negative) NO_y-induced ozone change for reasons similar to those indicated for the increasing HO_x case (see above). Many of the 2-D models used in the NASA HSRP/AESA assessment had a systematic bias, with ambient lower stratospheric O_3 levels greater than observed. Thus these models would be expected to have a bias, likely underpredicting ozone depletion for the HSCT scenario.

In conclusion, we expect to first order that models underestimating ambient NO_y concentrations in the lower stratosphere would generally predict systematically greater ozone column increases (or smaller depletions) in response to an HSCT perturbation, and that models overestimating ambient O_3 or H_2O would perform similarly. These sensitivity tests are useful in relating different model results, but they do not allow us to simply "fix" the HSCT assessment. For example, correcting the cause of why the GMI model underpredicts NO_y in the lower stratosphere may change more about the model atmosphere and how it handles HSCT perturbations than merely the NO_y profile.

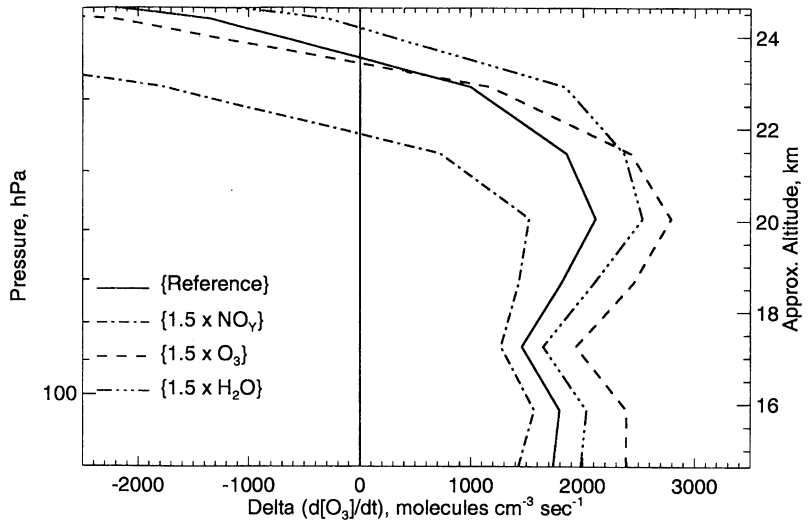

Figure 6. Box model calculation showing the change in ozone chemical tendency (Delta $d[O_3]/dt$) for a 10% increase in NO_y using July 15, 42°N conditions. Sensitivity scenarios are shown for different assumptions about the ambient abundance of NO_y, O_3, and H_2O. The reference scenario uses unmodified initial conditions from the GMI 3-D model. See text for details.

5.3. HSCT-Induced Ozone Change

The HSCT-induced change in the GMI model-derived midlatitude local ozone concentration at 42°N for the month of July is shown in Figure 7. The HSCT-induced ozone concentration change is positive below approximately 24 km: above this altitude level the perturbation is negative. Since the positive perturbation lobe is much greater than the negative perturbation lobe, the overall integrated column is positive at this latitude and season. This result is consistent with Figures 2 and 3. The large positive perturbation lobe could possibly be the result of CH_4-NO_x-HO_x smog chemistry [*Haagen-Schmit*, 1950; *Crutzen*, 1973]. Crutzen gave the first treatment of ozone formation in the global atmosphere via CH_4 oxidation. He considered radical attack on CH_4 to produce CH_3 followed by three reaction sequences that go from CH_3 to CO_2. Recently, *Johnston and Kinnison* [1998] extended Crutzen's approach including five significant branching points as methane is consumed, which includes 34 sequences (i.e., different reaction paths) to CO_2. The result of this work was a closed algebraic equation representing the net ozone tendency from the smog reactions. This approach is valid from the surface to the middle stratosphere (see *Poeschl et al.* [2000] and *Johnston and Kinnison* [2000] for more discussion on this approach). Applying this approach to the present study, using photochemical rates from the GMI model, gives results as shown in Figure 8. The solid line is the net ozone production from the smog reaction for the GMI reference atmosphere (subsonic only case). For comparison, the production of ozone from $2JO_2$ (twice the photolysis rate of molecular oxygen) is shown along with the total rate of ozone loss mediated from the NO_x family. It is important to note that the ozone change due to CH_4 is a net derivative and the ozone change mediated by the NO_x family is one component of

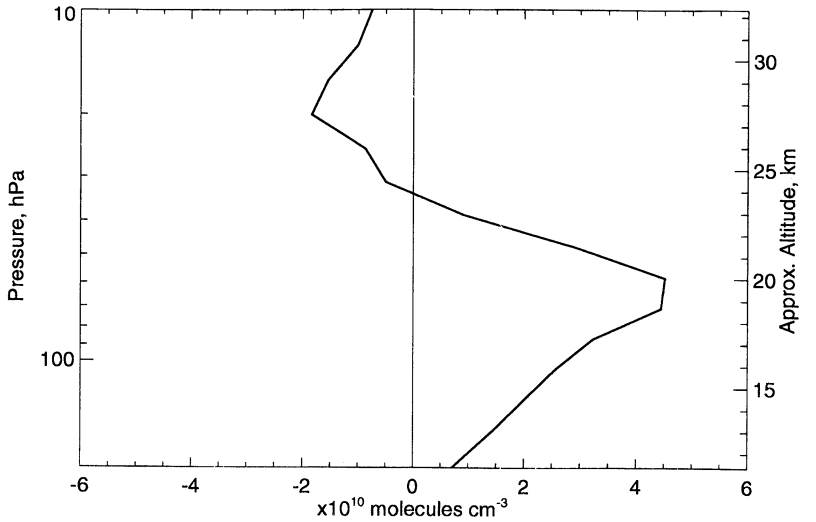

Figure 7. Calculated HSCT-induced change in ozone concentration (molecules cm^{-3}) at 42°N during July for the GMI model.

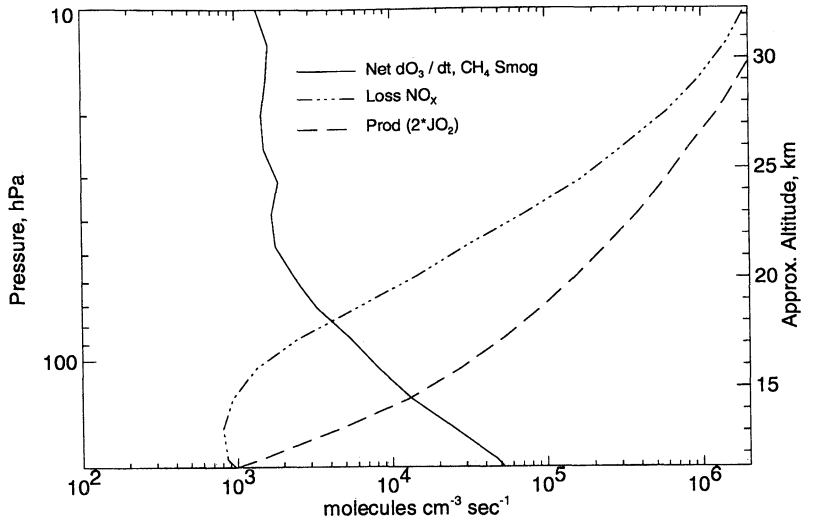

Figure 8. Calculated GMI 3-D model zonal average production and loss processes for ozone during July. The solid line is the net ozone production due to smog reactions for the base scenario. The long-dashed line represents the production of ozone from photolysis of oxygen. The dash-dotted line denotes the NO_X-catalyzed loss of ozone.

the total O_3 loss rate (i.e., total O_3 loss rate equal to Σ losses due to $NO_X + HO_X + ClO_X + BrO_X + O_X$). Keeping this in mind, it is interesting to note that the crossover point between the net change in ozone tendency from the CH_4 smog reactions versus the loss by NO_X processes is approximately 18 km at this latitude and season. In general, this model-derived crossover point has increased in altitude in recent years due to the inclusion of heterogeneous processes on sulfate aerosols (i.e., increased denoxification). Early work using a one-dimensional model with only gas-phase chemical processes had derived the crossover point to be approximately 13 km [*Johnston and Quitevis*, 1975]. The present result suggests that the aircraft addition of NO_X above 18 km (either from direct emission or transport from below) will most likely result in local ozone depletion; below this altitude, additional NO_X from aircraft will tend to produce ozone. However, the column ozone impact is not purely derived from local chemistry and will be sensitive to the transport of the NO_X, H_2O, and local ozone perturbations, affecting ozone at other altitudes, latitudes, and seasons.

There is a significant component of the HSCT-induced positive ozone perturbation lobe (as shown in Figure 7) that cannot be explained solely by CH_4-smog ozone production processes. This particular region is found between 24 and 18 km (at 42°N in July), and possibly several km lower, depending on exactly where the CH_4-smog processes become significant. The HSCT-induced increased ozone in this region can be explained by examining the interaction of both aircraft NO_X and H_2O (i.e., increased HO_X) on the local model-derived loss rates of ozone [*Wennberg et al.*, 1994; *Nevison et al.*, 1999]. Figure 9a shows the loss rate of ozone due to NO_X, HO_X, and the sum of the ClO_X-BrO_X families. At this latitude and season both the HO_X- and the ClO_X-BrO_X-mediated ozone losses are greater than that derived from the NO_X family, with the HO_X-related ozone loss representing the major mechanism for catalytic ozone removal in the lower stratosphere. At altitudes above 23 km the NO_X-catalyzed ozone loss is the dominant mechanism. Figure 9b shows the impact of a fleet of HSCTs emitting both NO_X and H_2O. The HSCT-induced change in the total O_3 loss rate (solid line) is negative below 22 km, inducing a positive change in ozone concentration in this region, as shown in Figure 7. The increase in ozone is due to the buffering of the HO_X and ClO_X-BrO_X ozone-catalyzed loss cycles by the added NO_X. Above 22 km the HSCT-induced total O_3 loss rate is positive, also consistent with the region where there is a decrease in local ozone concentration. In this region, the ozone concentration decrease is due to the increase in the NO_X-catalyzed loss rate.

The individual family terms for HSCT-induced total O_3 loss rates are also shown in Figure 9b. With the addition of HSCT NO_X and H_2O the total O_3 loss rate due to NO_X increases (dash-dotted line), and the HO_X (short-dashed line) and ClO_X-BrO_X (long-dashed line) loss rates generally decrease at all altitudes. It is easy to understand why the addition of HSCT NO_X increases the NO_X-catalyzed O_3 loss rate at all altitudes; however, it is not as straightforward to understand the overall decrease in the HO_X-catalyzed loss rate. Increases in local H_2O from HSCTs will tend to increase HO_X and should tend to increase the related HO_X-catalyzed O_3 loss. However, the added NO_X interference with the HO_X-catalyzed loss is greater than the direct contribution of added HO_X from H_2O. This effect was clarified via several sensitivity runs using the LLNL 2-D model [*Kinnison et al.*, 1994; *Kawa et al.*, 1999; *IPCC*, 1999] with three different HSCT emission assumptions (Figure 10). The solid line in Figure 10 shows the results of a 2-D model integration where both NO_X and H_2O are emitted. The HSCT-induced change in O_3 concentration is slightly positive below 17 km, with a more extensive negative peak above this altitude. The LLNL 2-D model gives an overall negative column ozone change at this latitude and season (not shown). When H_2O is the only emitted species, there is no positive lobe in the HSCT-induced change in O_3 concentration below 25 km. This is consistent with our understanding that as HSCTs increase the background H_2O, the HO_X abundance will increase, contributing more to the HO_X-catalyzed loss in the lower stratosphere. When NO_X is the only emitted species, there is a large positive lobe in HSCT-induced O_3 concentration below 24 km. In this case the NO_X interferes primarily with the HO_X-catalyzed O_3 loss and secondarily with the ClO_X-BrO_X-catalyzed O_3 loss, reducing the

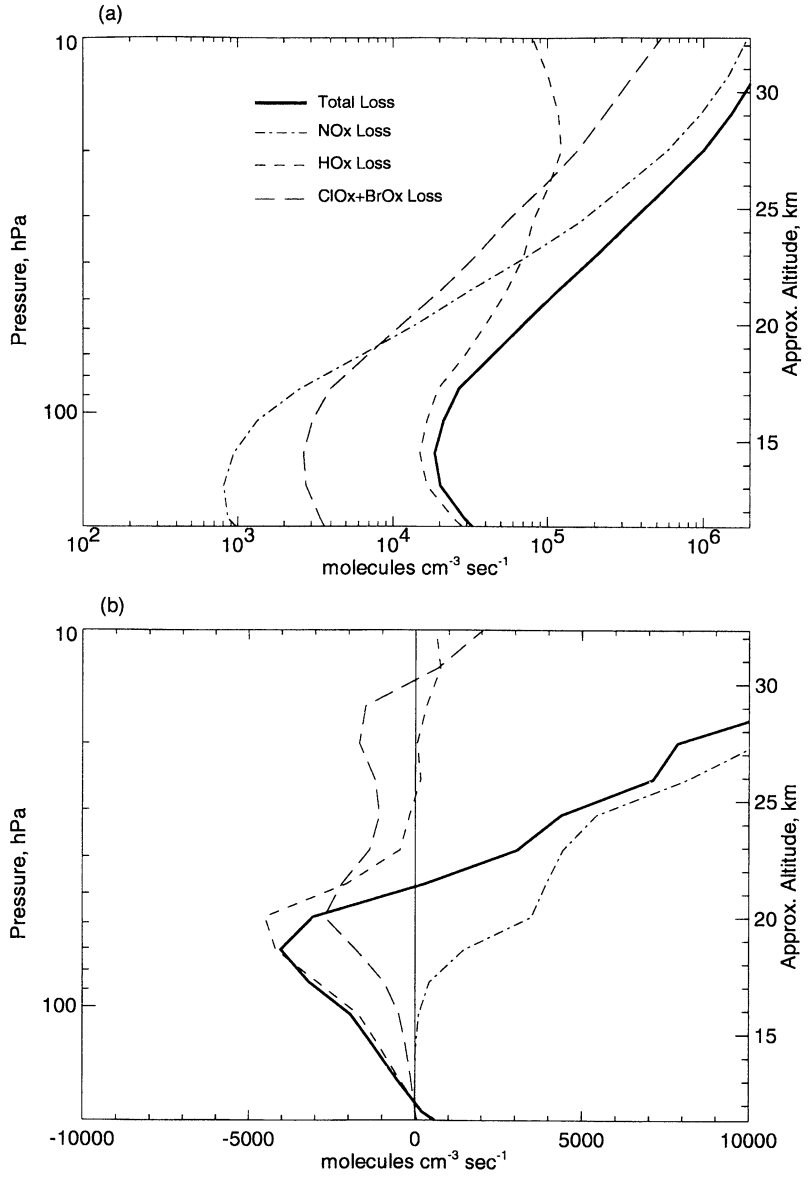

Figure 9. Ozone loss processes in the GMI 3-D model. Results are shown for the 2015 base atmosphere, which includes subsonic aircraft. (a) Individual and total (solid line) zonal average ozone loss rates at 42°N during July. (b) HSCT-induced change (i.e., the difference between the HSCT plus subsonic and subsonic only scenario) in the zonal average ozone loss rates for the individual families plus the total (solid line).

relative contribution of these latter O_3-catalyzed loss processes and increasing local ozone concentrations. In fact, if NO_X were not a component of HSCT engine effluent, the H_2O (i.e., HO_X) impact by itself would cause a much greater decrease in model-derived midlatitude, lower stratosphere local ozone than when NO_X emissions are included. The emitted NO_X acts as a buffer to the HO_X-induced HSCT-catalyzed ozone loss.

It is also interesting to compare the HSCT-induced O_3 concentration change between the GMI 3-D model (Figure 7) and LLNL 2-D model (Figure 10). The LLNL model has approximately twice the NO_Y in the lower stratosphere relative to the GMI model. Because of this, the LLNL 2-D model chemistry is more dominated by NO_X in the lower stratosphere and tends to give a more negative HSCT column ozone perturbation than that derived by the GMI 3-D model. However, it should be mentioned that the LLNL 2-D model overestimates the absolute abundance of ozone in the lower stratosphere. As discussed in section 5.2, this means that the LLNL 2-D model would still have a positive bias in the calculated HSCT impact on ozone. This points to the importance of considering a model's performance in simulating not only NO_Y, but also ozone (and water) in evaluating the assessment results.

5.4. Model Temperatures and the Impact on Polar Aerosol Chemistry

The Northern Hemisphere temperatures in the NCAR MACCM2 data set used to drive the GMI model are too warm compared with observations (see Figure 11), and thus the model does not predict the formation of polar stratospheric clouds (PSCs)

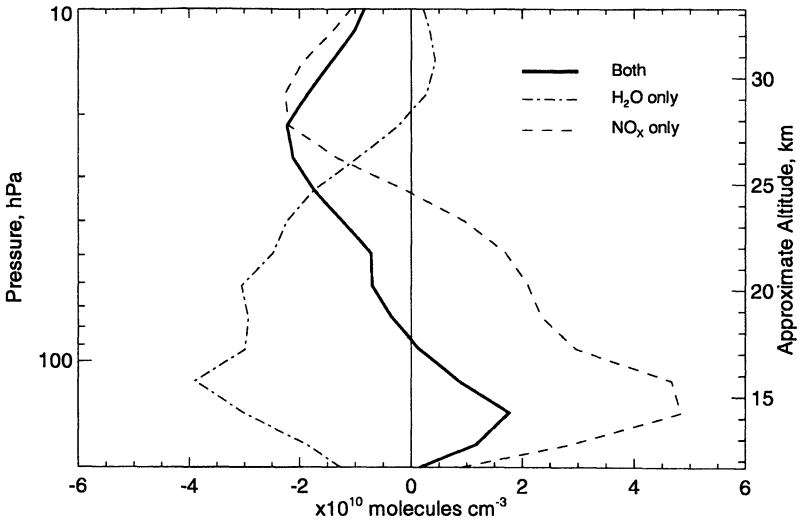

Figure 10. Calculated HSCT-induced change in ozone concentration (molecules cm^{-3}) at 42.5°N during July for the LLNL 2-D model for both H_2O and NO_y emissions (solid line), for H_2O only (dot-dashed line), and for NO_x only (dashed line).

during the winter. In this situation we cannot expect the impact of HSCTs on PSC occurrence and the resulting effects on O_3 concentrations to be realistic. However, temperatures in the Southern Hemisphere throughout the winter are in better agreement with observations, and we can examine the effects of HSCT emissions on the occurrence of PSCs and O_3 concentrations in the Southern Hemisphere vortex during winter and spring. Here we examine the 50-hPa level.

The Southern Hemisphere response to HSCT emissions depends on the transport characteristics of the model, particularly because HSCT emissions occur far from the Southern Hemisphere vortex. Global transport characteristics determine the fraction of HSCT emissions which eventually are transported into the Southern Hemisphere winter polar vortex. Prior to PSC formation in the Southern Hemisphere, HSCT-induced increases in H_2O and NO_y at 50 hPa were approximately 3.5% and 2.5%, respectively.

The larger amounts of H_2O and NO_y in the winter polar vortex raise PSC formation temperatures and result in the earlier occurrence of PSCs. As a result, the sedimentation of condensed-phase H_2O and HNO_3 also begins earlier. HSCT-induced increases in gas-phase H_2O are reduced from 3% to about 1% by mid-August, when PSC sedimentation is active. Increased H_2O from the HSCTs also allows more NO_y to be condensed into Type 1 PSCs and eventually on Type 2 PSCs. This results in a net decrease in gas-phase NO_y from June through mid-October, reaching a 1.5% decrease at the end of August.

HSCT emissions increase vortex-averaged Type 2 PSC SADs by 5-10% during July-September. Type 1 PSCs increase by similar amounts in June, but then give way to approximately 5% wintertime decreases compared to the reference atmosphere. This is probably due to increased condensation of NO_y onto Type 2 PSCs. In late winter when vortex temperatures increase, Type 1 PSC SADs are again larger when HSCT emissions are included.

The changes in gas-phase NO_y and PSC SADs mentioned above result in a small increase in active chlorine in the vortex at the end of the Southern Hemisphere winter. This produces a small decrease in lower stratospheric vortex ozone concentrations due to HSCTs of about 1% at the 50 hPa level at the end of October. See *Considine et al.* [2000] for an expanded discussion of the effects of HSCTs and polar processes in the GMI model.

The above discussion reflects the fact that, at least in the Southern Hemisphere, the net impact of HSCT exhaust on polar chemistry is a delicate balance of competing processes. This balance could easily change with slight changes in dynamics, temperature, or the treatment of denitrification and PSCs.

An important next step in the assessment of HSCT effects using the GMI model is to drive the model with a set of wind fields and temperatures having more realistic Northern Hemisphere temperatures in the polar vortex during winter. Much larger changes in NO_y and H_2O will be produced by HSCT emissions in the Northern Hemisphere in general (relative to the meteorological fields used in this study), although isolation of the vortex may limit the effects of HSCT emissions on ozone (see section 4.1). It is also important to test the adopted PSC mechanism by comparison to measurements in a specific year, by utilizing meteorological fields from an analysis (for example, Goddard GEOS products) for that year.

6. Conclusions

We have presented the results from a 3-D assessment of the impact of HSCTs on stratospheric ozone. This assessment examined the impact of a fleet of 500 HSCTs on the abundances of stratospheric ozone, NO_y, and H_2O. The total column ozone change in the Northern and Southern Hemisphere is +0.2% and +0.05%, respectively. These results exhibit a positive bias when compared with the central values adopted by the *IPCC* [1999] and HSRP [*Kawa et al.*, 1999] reports, but fall within the range of uncertainty suggested by the HSRP report. We have shown the relative importance of aircraft NO_x and H_2O effluent impacts on local and column ozone. Assuming an emission index (EI) NO_x of 5 g / kg fuel, the NO_x increases induced by the HSCT exhaust significantly buffer the ozone loss due to HO_x. We have also highlighted the importance of better understanding the processes that are responsible for polar ozone loss. The competing impacts of increased PSC sedimentation from a HSCT fleet are discussed.

As discussed in section 5.2, we believe that the GMI 3-D model clearly has systematic differences with respect to observations in the lower stratosphere. These errors most likely create a positive bias in the predicted ozone change. We emphasize that this

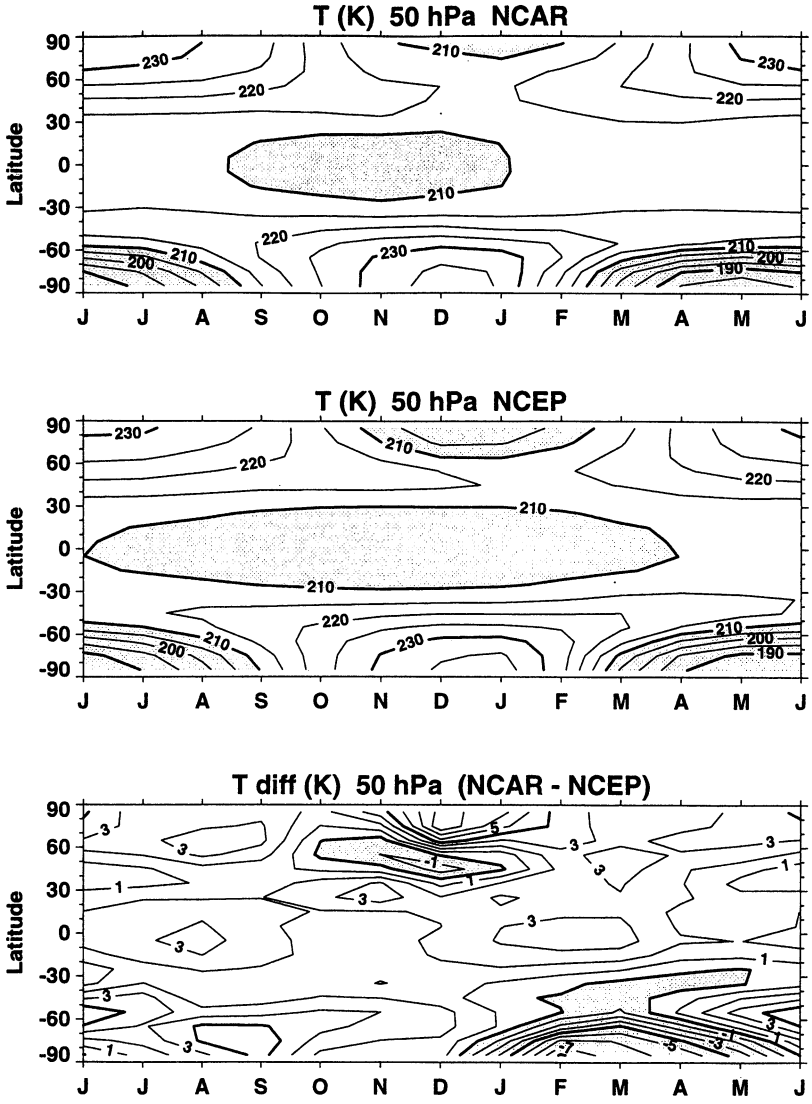

Figure 11. Comparison of the temperature distributions used in (top) the GMI model and (middle) the National Center for Environmental Prediction (NCEP) dataset. (bottom) Delta-temperature change (K) at 50 hPa between the two above mentioned distributions. The NCEP temperatures are representative of an 18-year climatology.

conclusion has been facilitated by comparison to other models and, more importantly, with pertinent atmospheric observations. Our analysis indicates that, besides testing of model results with observed NO_y and mean age of air derived from observations, it is also important to include the model's performance in comparisons with ozone and water. The GMI model performs very well in the comparison with ozone, while water has been constrained as much as possible using observations.

We expect an underestimation of the NO_y/H_2O exhaust accumulation, given the short calculated mean age of air. However, it is not possible at this point to quantify the relationship between exhaust accumulation and mean age of air. Furthermore, it is difficult to assess the impact of an increase in NO_y/H_2O exhaust accumulation, given the delicate balance between negative impacts above 25 km, and positive impact below. The magnitude of the positive response, and whether it increases or decreases with aircraft exhaust, will depend on where different grid points fall in the idealized curve presented by *Wennberg et al.* [1994].

It appears that the major reason for the outstanding discrepancies with mean age of air and NO_y (and N_2O) concentrations in the lower stratosphere is due to the model dynamics. This conclusion reflects correlated problems: merely correcting the mean age of air in the model does not mean that the transport has been "fixed." Indeed, different transport-related problems or other problems with the meteorological fields may arise. For example, we know that older versions of the MACCM2 [*Hall et al.*, 1999] give better agreement with the mean age of air, although their Southern Hemisphere temperatures are too low. This highlights a related problem with the MACCM2 fields: the tuning of the gravity wave parameterization, which improved Antarctic temperatures, leading in turn to a warm Arctic. It will be necessary to incorporate more realistic meteorological fields to improve the assessment. The Middle Atmosphere version of CCM3 (MACCM3) seems to have improved some of the problems in the earlier versions (P. Rasch, private communication, 2000) though it has yet to be tested for its behavior regarding mean age of air as well as NO_y and ozone. Other meteorological fields should also be tested. In this regard, the objective "grading" approach carried out by *Douglass et al.* [1999] provides an efficient and necessary (although not sufficient) first test of the

suitability of a given set of meteorological fields, before carrying out a full chemistry calculation.

The calculations carried out here have not included the possibility of small particles formed in the exhaust substantially increasing the sulfate aerosol surface area over most of the stratosphere [*Weisenstein et al.*, 1998]. In other model calculations the increase in stratospheric sulfate surface area has modified heterogeneous chemical processes and caused global-scale reductions in ozone [*Kawa et al.*, 1999]. Since the increases in surface area due to particle conversion in plumes could affect the ozone impact both at midlatitudes and in the polar vortices, it is important that a 3-D model should eventually include a self-consistent calculation of the sulfate aerosol microphysics.

These calculations have not included new and updated chemistry, which has been recently suggested [*Brown et al.*, 1999; *Dransfield et al.*, 1999] to explain the discrepancy in NO_x/NO_y ratios observed during the Photochemistry of Ozone Loss in the Arctic Region in Summer (POLARIS) campaign. Including these updates will tend to increase the NO_x/NO_y ratio, which would tend to make the HSCT delta-ozone impact more negative (or less positive).

Finally, it should be stated that this HSCT assessment used a proposed fleet size of 500 aircraft and an EI NO_x of 5 g/kg fuel. Future fleets could have a greater number of aircraft (e.g., 1000) and potentially a larger emission index for NO_x (e.g., EI NO_x of 5-15 g/kg fuel). Both of these conditions would make the HSCT delta-ozone impact more negative (or less positive). In addition, 2-D model studies have shown that the calculated ozone impact is sensitive to the assumed supersonic cruise altitudes. Thus the ozone impact is expected to be sensitive to the speed and design of any future supersonic transports. Sensitivity studies addressing these issues have been carried out in detail by both *Kawa et al.*, [1999] and *IPCC* [1999].

Acknowledgments. The National Center for Atmospheric Research is operated by the University Corporation for Atmospheric Research under the sponsorship of the National Science Foundation. Douglas Kinnison was supported through a subcontract (B505190) between NCAR and Lawrence Livermore National Laboratory. The work at LLNL was supported by NASA AEAP contract S-10173-X. Work at Lawrence Livermore National Laboratory was performed under the auspices of the U.S. Department of Energy under contract W-7405-Eng-48.

References

Avallone, L. M., and M. J. Prather, Tracer-tracer correlations: Three-dimensional model simulations and comparison to observations, *J. Geophys. Res.*, *102*, 19,233-19,246, 1997.

Baughcum, S. L., and S. C. Henderson, Aircraft emission inventories projected in year 2015 for a High Speed Civil Transport (HSCT) universal airline network, *NASA Contract. Rep., CR-4659*, 1995.

Baughcum, S. L., and S. C. Henderson, Aircraft emission scenarios projected in year 2015 for the NASA Technology Concept Aircraft (TCA) High Speed Civil Transport, *NASA Contract. Rep., CR-1998-207635*, 1998.

Baughcum, S. L., S. C. Henderson, and D. J. Sutkus, Scheduled civil aircraft emission inventories projected for 2015: Database development and analysis, *NASA Contract. Rep., CR-1998-207638*, 1998.

Boering, K. A., S. C. Wofsy, B. C. Daube, H. R. Schneider, M. Loewenstein, J. R. Podolske, and I. J. Conway, Stratospheric mean ages and transport rates from observations of carbon dioxide and nitrous oxide, *Science*, *274*, 1340-1343, 1996.

Boville, B. A., Middle atmosphere version of the CCM2 (MACCM2): Annual cycle and interannual variability, *J. Geophys. Res.*, *100*, 9017-9040, 1995.

Brasseur, G., G. T. Amanatidis, and G. Angeletti, European scientific assessment of the atmospheric effects of aircraft emissions, *Atmos. Environ.*, *32*, 2327-2422, 1998.

Brown, S. S., R. K. Talukdar, and A. Ravishankara, Rate constants for the reaction $OH + NO_2 + M \rightarrow HNO_3$ under atmospheric conditions, *Chem. Phys. Lett.*, *299*, 277-284, 1999.

Climatic Impact Assessment Program (CIAP), Report of findings: The effects of stratospheric pollution by aircraft, edited by A. J. Grobecker, S. C. Coroniti, and R. H. Cannon Jr., *Rep. DOT-TST-75-50*, 551 pp., U.S. Dep. of Transp., Washington, D. C., 1974.

Climatic Impact Assessment Program (CIAP), Propulsion effluent in the stratosphere, *Monogr. 2*, U.S. Dep. of Transp., Washington, D. C., 1975a.

Climatic Impact Assessment Program (CIAP), The stratosphere perturbed by propulsion effluent, *Monogr. 3*, U.S. Dep. of Transp., Washington, D. C., 1975b.

Considine, D. B., A. R. Douglass, P. S. Connell, D. E. Kinnison, and D. A. Rotman, A polar stratospheric cloud parameterization for the three-dimensional model of the Global Modeling Initiative and its response to stratospheric aircraft, *J. Geophys. Res.*, *105*, 3955-3975, 2000.

Crutzen, P. J., A discussion of some minor constituents in the stratospheric and troposphere, *Pure Appl. Geophys.*, *106*, 1385-1399, 1973.

DeMore, W. B., S. P. Sander, D. M. Golden, R. F. Hampson, M. J. Kurylo, C. J. Howard, A. R. Ravishankara, C. E. Kolb, and M. J. Molina, Chemical kinetics and photochemical data for use in stratospheric modeling, NASA panel for data evaluation, number 12, *JPL Publ., 97-4*, 1997.

Douglass, A. R., and S. R. Kawa, Contrast between 1992 and 1997 high-latitude spring Halogen Occultation Experiment observations of lower stratospheric HCl, *J. Geophys. Res.*, *104*, 18,739-18,754, 1999.

Douglass, A. R., M. A. Carroll, W. B. DeMore, J. R. Holton, I. S. A. Isaksen, and H. S. Johnston, The Atmospheric Effects of Stratospheric Aircraft: A current consensus, *NASA Ref. Publ., 1251*, 1991.

Douglass, A. R., M. P. Prather, T. M. Hall, S. E. Strahan, P. J. Rasch, L. C. Sparling, L. Coy, and J. M. Rodriguez, Choosing meteorological input for the Global Modeling Initiative assessment of high speed aircraft, *J. Geophys. Res.*, *104*, 27,545-27,564, 1999.

Dransfield, T. J., K. K. Perkins, N. M. Donahue, J. G. Anderson, M. M. Sprengnether, and K. L. Demerjian, Temperature and pressure dependent kinetics of the gas-phase reaction of the hydroxyl radical with nitrogen dioxide, *Geophys. Res. Lett.*, *26*, 687-690, 1999.

Haagen-Smit, A. J., The air pollution problem in Los Angeles, *Eng. Sci.*, *14*, 7-13, 1950.

Hall, T. M., and D. W. Waugh, Stratospheric residence time and its relationship to mean age, *J. Geophys. Res.*, *105*, 6773-6782, 2000.

Hall, T. M., D. W. Waugh, K. A. Boering, and R. A. Plumb, Evaluation of transport in stratospheric models, *J. Geophys. Res.*, *104*, 18,815-18,839, 1999.

Intergovernmental Panel on Climate Change (IPCC), *Climate Change 1995: The Science of Climate Change*, edited by J. T. Houghton et al., Cambridge Univ. Press, New York, 1996.

Intergovernmental Panel on Climate Change (IPCC), *Aviation and the Global Atmosphere*, edited by J. E. Penner et al., Cambridge Univ. Press, New York, 1999.

Jackman, C. H., E. L. Fleming, S. Chandra, D. B. Considine, and J. E. Rosenfield, Past, present, and future modeled ozone trends with comparisons to observed trends, *J. Geophys. Res.*, *101*, 28,753-28,767, 1996.

Johnston, H. S., Reduction of stratospheric ozone by nitrogen oxide catalysts from supersonic transport exhaust, *Science*, *173*, 517-522, 1971.

Johnston, H. S., and D. E. Kinnison, Methane photooxidation in the atmosphere: Contrast between two methods of analysis, *J. Geophys. Res.*, *103*, 21,967-21,984, 1998.

Johnston, H. S., and D. E. Kinnison, Reply to comment by U. Poeschl, M. G. Lawrence, R. von Kahlmann, and P. J. Crutzen,, *J. Geophys. Res.*, *105*, 1435-1439, 2000.

Johnston, H. S., and E. Quitevis, The oxides of nitrogen with respect to urban smog, supersonic transports, and global methane, in *Radiation Research*, edited by O. B. Nygaard, H.I. Adler, and W.K. Sinclair, pp. 1299-1313, Academic, San Diego, Calif., 1975.

Johnston, H. S., D. E. Kinnison, and D. J. Wuebbles, Nitrogen oxides from high-altitude aircraft: An update of potential effects on ozone, *J. Geophys. Res.*, *94*, 16,351-16,363, 1989.

Johnston, H. S., M. J. Prather, and R. T. Watson, The Atmospheric Effects

of Stratospheric Aircraft: A topical review, *NASA Ref. Pub., 1250*, 1991.

Kasten, F., Falling speed of aerosol particles, *J. Appl. Meteorol., 7*, 944-947, 1968.

Kawa, S. R., et al., Assessment of the effects of high-speed aircraft in the stratosphere: 1998, *NASA Tech. Pap., TP-1999-209237*, 1999.

Kinnison, D.E., K.E. Grant, P.S. Connell, D.A. Rotman, and D.J. Wuebbles, The chemical and radiative effects of the Mt. Pinatubo eruption, *J. Geophys. Res., 99*, 25,705-25,731, 1994.

Lin, S. J., and R. B. Rood, Multidimensional flux form semi-Lagrangian transport schemes, *Mon. Weather Rev., 124*, 2046-2070, 1996.

Logan, J. A., An analysis of ozonesonde data for the lower stratosphere: Recommendations for testing models, *J. Geophys. Res., 104*, 16,151-16,170, 1999.

Mortlock, A. M., and R. van Alstyne, Military, charter, unreported domestic traffic and general aviation: 1976, 1984, 1992, and 2015 emission scenarios, *NASA Contract. Rep., CR-1998-207639*, 1998.

National Academy of Sciences (NAS), *Environmental Impact of Stratospheric Flight*, 348 pp., Washington, D. C., 1975.

National Research Council, *U.S. Supersonic Commercial Aircraft: Assessing NASA's High Speed Research Program*, Natl. Acad. Press, Washington, D. C., 1997.

National Research Council, *A Review of NASA's Atmospheric Effects of Stratospheric Aircraft Project*, Natl. Acad. Press, Washington, D. C., 1999.

Nevison, C. D., S. Solomon, and R. S. Gao, Buffering interactions in the modeled response of stratospheric O_3 to increased NO_X and HO_X, *J. Geophys., Res., 104*, 3741-3754, 1999.

Park, J., M. K. W. Ko, C. H. Jackman, R. A. Plumb, A. Kaye, and K. H. Sage (Eds.), Models and Measurements Intercomparison II, *NASA Tech. Memo., TM-1999-209554*, 1999.

Poeschl, U., M. G., Lawrence, R. von Kahlmann, and P. J. Crutzen, Comment on "Methane photooxidation in the atmosphere: Contrast between two methods of analysis" by H. Johnston and D. Kinnison, *J. Geophys.* Res., *105*, 1431-1433, 2000.

Prather, M. J., and E. E. Remsberg (Eds.), The Atmospheric Effects of Stratospheric Aircraft: Report of the 1992 Models and Measurements Workshop, *NASA Ref. Publ., 1292*, 1993.

Prather, M. J., H. L. Wesoky, R. C. Miake-Lye, A. R. Douglass, R. P. Turco, D. Wuebbles, M. K. W. Ko, and A. L. Schmeltekopf, The Atmospheric Effects of Stratospheric Aircraft: A first program report, *NASA Ref. Publ., 1272*, 1992.

Ramaroson, R., Local, one and three-dimensional modeling of chemical processes in the middle atmosphere, Ph.D thesis, Univ. Paris VI, Paris, France, 1989.

Rasch, P. J., X. Tie, B. A. Boville, and D. L. Williamson, A three-dimensional transport model for the middle atmosphere, *J. Geophys. Res., 99*, 999-1017, 1994.

Rasch, P. J., B. A. Boville, and G. P. Brasseur, A three-dimensional general circulation model with coupled chemistry for the middle atmosphere, *J. Geophys. Res., 100*, 9041-9071, 1995.

Rodriguez, J. M., Global Modeling Initiative, *NASA Ref. Publ., 1385*, 1996.

Rotman, D. A., et al., Global Modeling Initiative assessment model: Model description, integration and testing of the transport shell, *J. Geophys. Res.*, this issue.

Salawitch, R. J., et al., The distribution of hydrogen, nitrogen, and chlorine radicals in the lower stratosphere: Implications for changes in O_3 due to emission of NO_y from supersonic aircraft, *Geophys. Res. Lett., 21*, 2547-2550, 1994.

Stolarski, R. S., and H. L. Wesoky, The Atmospheric Effects of Stratospheric Aircraft: A second program report, *NASA Ref. Publ., 1293*, 1993a.

Stolarski, R. S., and H. L.Wesoky, The Atmospheric Effects of Stratospheric Aircraft: A third program report, *NASA Ref. Publ., 1313*, 1993b.

Stolarski R. S., and H. L. Wesoky, The Atmospheric Effects of Stratospheric Aircraft: A fourth program report, *NASA Ref. Publ., 1359*, 1995.

Stolarski, R. S., et al., 1995 scientific assessment of the Atmospheric Effect of Stratospheric Aircraft, *NASA Ref. Publ., 1381*, Washington, D. C., 1995.

Strahan, S., and J. D. Mahlman, Evaluation of the SKYHI general circulation model using aircraft N_2O measurements, 1, Polar winter stratospheric meteorology and tracer meteorology, *J. Geophys. Res., 99*, 10,305-10,318, 1994.

Strahan, S. E., M. Loewenstein, and J. R. Podolske, Climatology and small-scale structure of lower stratospheric N_2O based on in situ observations, *J. Geophys. Res., 104*, 2195-2208, 1999.

Waugh D.W., et al., Three-dimensional simulations of long-lived tracers using winds from MACCM2, *J. Geophys. Res., 102*, 2,1493-21,513, 1997.

Weisenstein, D. K., M. K. W. Ko, I. G. Dyominov, G. Pitari, L. Ricciardulli, G. Visconti, and S. Bekki, The effects of sulfur emissions from HSCT aircraft: A 2-D model intercomparison, *J. Geophys. Res., 103*, 1527-1547, 1998.

Wennberg, P. O., et al., The removal of lower stratospheric O_3 by free radical catalysis: In situ measurements of OH, HO_2, NO, NO_2, ClO, and BrO, *Science, 266*, 398-404, 1994.

World Meteorological Organization (WMO), Scientific assessment of ozone depletion: 1991, *Rep. 25*, Global Ozone Res. and Monit. Proj., Geneva, 1992.

World Meteorological Organization (WMO), Scientific assessment of ozone depletion: 1998, *Rep. 44*, Global Ozone Res. and Monit. Proj., Geneva, 1999.

S. L. Baughcum, Boeing Company, P. O. Box 3707, Seattle, WA 98124-2207.

P. S. Connell, D. A. Rotman, and J. Tannahill, Lawrence Livermore National Laboratory, L-103, 7000 East Ave., Livermore, CA 94550.

D. B. Considine, L. Coy, A. R. Douglass, and S. R. Kawa, NASA Goddard Space Flight Center, Mail Code 916, Greenbelt Rd., Greenbelt, MD 20771-0001.

D. E. Kinnison and P. J. Rasch, National Center for Atmospheric Research, P. O. Box 3000, Boulder, CO 80307-3000. (dkin@acd.ucar.edu)

M. J. Prather, Department of Earth System Science, University of California at Irvine, Irvine, CA 92697-3100.

R. Ramaroson, Office National d'Etudes et Recherches Aerospatiales, 92322 Chatillon, France.

J. M. Rodriguez, Department of Marine and Atmospheric Chemistry, University of Miami, 4600 Rickenbacker Causeway, Miami, FL 33149-1098.

D. W. Waugh, Department of Earth and Planetary Sciences, The Johns Hopkins University, 320 Olin Hall, 3400 N. Charles St., Baltimore, MD 91109-8099.

(Received April 20, 2000; revised June 26, 2000;
accepted June 29, 2000.)